JOURNAL OF GEOPHYSICAL RESEARCH, VOL. 113, D08203, doi:10.1029/2007JD009147, 2008

Stratospheric impact of the Chisholm pyrocumulonimbus eruption: 2. Vertical profile perspective

M. Fromm,[1] E. P. Shettle,[1] K. H. Fricke,[2] C. Ritter,[3] T. Trickl,[4] H. Giehl,[4] M. Gerding,[5] J. E. Barnes,[6] M. O'Neill,[6] S. T. Massie,[7] U. Blum,[8] I. S. McDermid,[9] T. Leblanc,[9] and T. Deshler[10]

Received 10 July 2007; accepted 8 January 2008; published 17 April 2008.

[1] Extreme pyrocumulonimbus (pyroCb) blowups that pollute the stratosphere have been documented on at least five occasions. However, the frequency of these events is still uncertain. One published pyroCb case study, the Chisholm Fire in May 2001, was restricted to the convective phase and its immediate aftermath. Here and in a companion paper we describe the stratospheric impact of the Chisholm pyroCb. The companion paper focuses on nadir satellite views of the plume. This paper synthesizes a broad array of space-, balloon-, and ground-based profile measurements. The Chisholm pyroCb, which we identify as the singular cause of stratospheric aerosol increase in northern spring/summer of 2001, created a doubling of the zonal average aerosol optical depth in the lowermost stratosphere. The meridional spread of the plume was from the tropics (20°N) to the high Arctic (79°N) within the first month. The stratospheric Chisholm smoke became a hemispheric phenomenon in midlatitudes and northern tropics and persisted for at least 3 months. A size-resolved particle concentration profile over Laramie, Wyoming, indicated a lower stratospheric aerosol with a twofold to threefold increase in volume of particles with radii between 0.3 and 0.6 μm. We also find evidence of localized warming in the air masses of four of the lidar-measured smoke layers. This work contains the first reported stratospheric smoke layers measured by lidar at Ny Ålesund, Esrange, Kühlungsborn, Garmisch-Partenkirchen, Boulder, and Mauna Loa. In addition, the first detection of smoke-enhanced aerosol extinction at near IR wavelengths by the Halogen Occultation Experiment (HALOE) is introduced.

Citation: Fromm, M., et al. (2008), Stratospheric impact of the Chisholm pyrocumulonimbus eruption: 2. Vertical profile perspective, *J. Geophys. Res.*, *113*, D08203, doi:10.1029/2007JD009147.

1. Introduction

[2] Explosive convection has been observed and theorized to have global impact on the stratosphere, and consequently climate. The ''standard'' process for sudden injection of aerosols and gases through the tropopause is a volcanic eruption [*Brasseur and Solomon*, 1986], a predominantly convective phenomenon. Plinian volcanic thrusts involve entrainment of ambient air into the lower column, and gain buoyancy from the release of latent heat as abundant water vapor condenses when the rising column cools [*Sigurdsson et al.*, 2000]. Such injections can have a substantial global temperature impact [e.g., *Labitzke and McCormick*, 1992].

[3] The Nuclear Winter hypothesis [*Crutzen and Birks*, 1982; *Turco et al.*, 1983] stimulated intensive exploration into observations of strong pyroconvection of smoke and pollutants into the lower stratosphere [e.g., *Pyne and Omi*, 1986; *Stocks and McRae*, 1991]. The stratospheric lifetime of the gases and particles from a nuclear war would be long, increasing the potential for widespread and long-lasting thermodynamic and/or chemical impact. Important findings implicating extreme air mass convection and pyroconvection in the transport of boundary layer material into the lowermost stratosphere were reported by *Poulida et al.* [1996] and *Waibel et al.* [1999], respectively. With the aid of abundant profiles of aerosol extinction by the Polar Ozone and Aerosol Measurement (POAM) III [*Lucke et al.*, 1999] and Stratospheric Aerosol and Gas Experiment (SAGE) II [*Mauldin et al.*, 1985] satellite instruments, the

[1]Naval Research Laboratory, Washington, D. C., USA.
[2]Physikalisches Institut, Universität Bonn, Bonn, Germany.
[3]Alfred-Wegener Institute for Polar- and Marine Research, Potsdam, Germany.
[4]IMK-IFU, Forschungszentrum Karlsruhe, Garmisch-Partenkirchen, Germany.
[5]Leibniz-Institute of Atmospheric Physics, Kühlungsborn, Germany.
[6]Global Monitoring Division, NOAA, Boulder, Colorado, USA.
[7]Atmospheric Chemistry Division, National Center for Atmospheric Research, Boulder, Colorado, USA.
[8]Forsvarets Forskningsinstitutt, Kjeller, Norway.
[9]Table Mountain Facility, Jet Propulsion Laboratory, California Institute of Technology, Wrightwood, California, USA.
[10]Department of Atmospheric Science, University of Wyoming, Laramie, Wyoming, USA.

0148-0227/08/2007JD009147$09.00

Table 1. Summary of Aerosol Lidar Instruments and Dates of Measurements Presented in This Paper

Location	Latitude (°N)	Longitude (+°E; −°W)	Wavelength (nm)	Measurement Dates
Ny Ålesund	78.9	13.9	532	11 May, 24 and 29 Jun
Esrange	67.9	21.1	532	25–28 Jul, 3 and 14 Aug
Kühlungsborn	54.1	11.8	532	9 Jul
Garmisch-Partenkirchen	47.5	11.1	532	2 May; 12, 23, and 26 Jun; 3 Jul
Boulder	40.0	−105.0	532	8, 9, 13, and 23 May; 1, 15, 16, 23, 29 Jun; 15, 17, and 28 Jul; 8 and 17 Aug
Mauna Loa (NOAA)	19.5	−155.6	355	2, 10, 24, and 30 May; 21 and 26 Jun; 18 and 24 Jul; 3, 8, 15, 23, and 29 Aug
Mauna Loa (JPL)	19.5	−155.6	532	5, 8–10, 15, 18, 22, 24–26, 30, and 31 May; 2, 4, 5, 12, 15, 16, 26, 27, and 30 Jun; 7, 10, 13, 14, 17–20, 23, 24, 27, and 31 Jul; 1–4, 8–10, 14, 15, 17, 18, 21, 24, 25, 28, and 30 Aug

first-ever linking of widespread stratospheric smoke with so-called pyrocumulonimbus (pyroCb for short) was reported by *Fromm et al.* [2000] and *Fromm and Servranckx* [2003] (hereinafter referred to as FS03). Since then *Livesey et al.* [2004], *Jost et al.* [2004], and *Fromm et al.* [2006] revealed a similar cause and effect for pyroCb events in 1992, 2002, and 2003 (in the Southern Hemisphere), respectively. Hence it is becoming increasingly evident that pyroconvection with an impact on the upper troposphere and lower stratosphere (UTLS) occurs with a frequency that is important, yet still poorly characterized [*Fromm et al.*, 2004].

[4] To characterize the stratospheric impact of the Chisholm pyroCb described in the above papers, we present here a wide range of profile measurements that record the abundance, vertical extent, horizontal spread, and persistence of the Chisholm stratospheric smoke plume. A companion paper [*Fromm et al.*, 2008] (hereinafter referred to as F08) describes the plume as observed by nadir-viewing satellite instruments including the Total Ozone Monitoring Spectrometer (TOMS) aerosol index (AI) in the first week after injection. Herein we invoke the AI, but otherwise limit the analysis to vertical profiles.

2. Data

2.1. Solar Occultation (SO)

[5] POAM III version 4 aerosol extinction profiles (see *Randall et al.* [2001] and *Russell et al.* [2005] for a validation/comparison studies) have been used for analysis of background aerosols, volcanic plumes [*Rose et al.*, 2003], and polar stratospheric clouds (PSC) [*Bevilacqua et al.*, 2002; *Fromm et al.*, 2003; *Palm et al.*, 2005; *Alfred et al.*, 2007; *Daerden et al.*, 2007], in addition to the above mentioned stratospheric smoke. Individual profiles of aerosol extinction have an uncertainty of ∼10% in the upper troposphere and lower stratosphere (UTLS) [*Randall et al.*, 2001]. In the Northern Hemisphere spring and summer, the period of study, POAM III's measurement latitude is nearly invariant on a daily basis, starting at ∼55°N in May, reaching minimum ∼54°N at solstice, and increases to ∼65°N by September.

[6] Stratospheric Aerosol and Gas Experiment (SAGE) II aerosol extinction profiles have been used in a wealth of applications over its years of operation (1984–2005). For instance, *Thomason et al.* [1997] used SAGE II extinction coefficient for a global stratospheric aerosol climatology; *Rizi et al.* [2000] analyzed the plume from the eruption of Shishaldin volcano in April 1999; *Wang et al.* [1994] presented a climatology of subvisual cirrus (SVC); *Palm et al.* [2005] showed SAGE II–measured Antarctic PSCs in 2003; and *Fromm et al.* [2000] showed both SAGE II and POAM III smoke layers in the lowermost stratosphere in boreal summer 1998. In the northern spring/summer SAGE II sweeps rapidly/episodically through mid and high latitudes, creating a seasonal pattern characterized by brief periods of measurements with slightly longer gaps in between. In northern summer 2001 SAGE II midlatitude and high-latitude measurements were only available for roughly 1-week periods early in May, June, July, and August. In this work we use SAGE II profiles poleward of 25°N.

[7] HALOE [*Russell et al.*, 1993] aboard the Upper Atmosphere Research Satellite (UARS) [*Reber et al.*, 1993] operated from September 1991 until December 2005. Over this span HALOE delivered an impressively continuous and stable record of aerosol extinction coefficient at four near infrared wavelengths (2.54, 3.40, 3.46, and 5.25 μm). *Hervig* [1999] analyzed a PSC observed by HALOE over the United Kingdom in March 1996. *Hervig and McHugh* [1999] also used the multiple aerosol extinction wavelengths to analyze and model the characteristics of SVC.

2.2. Lidar

[8] We assembled measurements of enhanced aerosols in the lowermost stratosphere from seven lidar instruments. The locations and basic characteristics are listed in Table 1. The search for applicable measurements included searching the NDACC (Network for the Detection of Atmospheric Composition Change, formerly named the Network for the Detection of Stratospheric Change (NDSC)) and consulting instrument principal investigators. The list below represents those data sets offered for this study that had any UTLS measurements between May and August 2001.

2.2.1. Ny Ålesund

[9] Lidar data from Spitsbergen were obtained by the Koldewey Aerosol Raman Lidar which is located in Ny Ålesund at 78.9°N and 13.9°E at the west coast of Spitsbergen. The lidar is integrated in the NDACC station and consisted at that time of a Nd:YAG laser operating at 1064 nm

and 532 nm with 30 Hz repetition rate and about 150 mJ pulse energy. Signals for this work have been collected by a 30 cm Zerodur mirror with a field of view of 0.83 mrad. More information regarding the system is given by *Ritter et al.* [2004].

[10] In this work data have been averaged over 60 m in space and around 11 min in time. The aerosols were retrieved according to *Klett* [1985] with a lidar ratio (ratio between aerosol extinction and backscatter) of 30 sr in the stratosphere. The necessary boundary condition was chosen to be: average backscatter ratio = 1.05 in an interval between 18 and 21 km. Hence, the altitude where the boundary condition was applied is located at least 4 km above the presented smoke layers to decrease the influence of the choice of the boundary condition.

[11] At 14 km altitude the signal-to-noise ratio of the lidar profile is roughly 25, giving rise to an uncertainty of the backscatter ratio of ±0.02 per height increment (10 min temporal and 60 m spatial resolution).

2.2.2. Esrange

[12] The University of Bonn lidar at Esrange in northern Sweden (68°N, 21°E) is optimized for operating at a wavelength of 532 nm. The beam direction is fixed vertically and the atmosphere echo is recorded with counting electronics on a 150-m grid for both parallel and perpendicular polarizations during day and nighttime operations. In darkness the return from the vibrational Raman scattering on N_2 molecules and the return at 1064 nm are also recorded. The power aperture product is 7 W m^{-2}. With a clear boundary layer a net signal from 80 km altitude is obtained in 5 min of integration time in darkness. The polarization measurements discriminate rotationally symmetric scatterers (e.g., liquid droplets) from asymmetric scatterers (solid particles). Technical and performance details for this lidar have been described by *Blum and Fricke* [2005].

2.2.3. Kühlungsborn

[13] The Rayleigh/Mie/Raman (RMR) lidar at Kühlungsborn, Germany (54°N, 12°E) is designed for the observation of aerosol parameters like backscatter ratio or backscatter coefficient [*Alpers et al.*, 1999], since summer 2002 complemented by temperature profiles derived from a combination of Rayleigh and Raman backscatter measurements [*Alpers et al.*, 2004; *Rauthe et al.*, 2006]. It uses an injection seeded Nd:YAG laser as the lidar transmitter. The laser simultaneously emits the fundamental wavelength (1064 nm) as well as the second and third harmonic wavelengths (532 and 355 nm). The pulse energies are 500, 400, and 200 mJ, respectively, and the pulse repetition rate is 30 Hz. In this study, only the backscatter at 532 nm is examined. For the signal detection two telescopes with parabolic principal mirrors of 50 cm diameter are used. One of the mirrors is equipped with a polarizer plate that is adjusted perpendicular to the polarization plane of the 532 nm laser light. The backscattered photons are preintegrated over 4000 laser pulses (about 2.5 min). Further integration is applied depending on the purpose. The altitude resolution is 50 m. For the calculation of backscatter ratios we use the N_2 vibrational Raman signal at 387 nm as measure of the pure molecular signal. The Raman signal is normalized to the elastic signal in the altitude range of 28.5 to 30.5 km or 17.0 to 20.0 km for the unpolarized or cross-polarized backscatter at 532 nm, respectively. The backscatter ratio is smoothed with a ±10 bin Hanning window.

[14] Most of the soundings in summer 2001 were performed for tropospheric aerosol detection [*Schneider and Eixmann*, 2002], the others for the examination of noctilucent clouds in the mesosphere [*Alpers et al.*, 2000]. A limited number of observations focus on the UTLS. In this study only the latter can be used for quantitative studies. The mesospheric studies provide only qualitative information in the lowermost stratosphere because the signal is partly blocked by a chopper, inhibiting quantitative analysis below about 18 km.

[15] The radiosonde data are from the routine operations of the German Weather Service at Lindenberg (52°N, 14°E, ~261 km from the lidar site). Out of the four daily launches we have chosen the midnight launch because it is closest to the time of the lidar soundings. The radiosonde data are available with a height resolution of 50 m, and the temperature error is less than 0.2 K in the region below 20 km. The tropopause is defined as the altitude where the temperature gradient is larger than −2 K/km for at least 2 km.

2.2.4. Garmisch-Partenkirchen

[16] The aerosol lidar at Garmisch-Partenkirchen (47.5°N, 11.1°E) was built in 1973 and 1974. Quantitative data were first retrieved in 1976. This has yielded one of the longest records of the stratospheric aerosol [*Jäger*, 2005; *Deshler et al.*, 2006]. In 1990/1991 high-resolution angular scanning was introduced for the investigation of contrails [*Freudenthaler et al.*, 1994], and the ruby laser (694.3 nm) was replaced by a more powerful, frequency-doubled Nd:YAG laser (Quanta Ray, GCR-4). The laser transmits 550 mJ at 532 nm, with a 10-Hz repetition rate, in combination with the original 0.52-m-diameter receiver. The upgraded system subsequently became a primary instrument of the NDACC network.

2.2.5. Mauna Loa (JPL)

[17] The JPL lidar at Mauna Loa Observatory (MLO) was installed in 1993. It makes nighttime measurements averaged over 2 h, usually beginning at the end of astronomical twilight, and 3–4 nights per week on average. While it is primarily an ozone and temperature lidar system for measurements in the upper troposphere and above, good aerosol backscatter measurements at 355 nm are also obtained. At 355 nm the lidar transmits >120 mJ per pulse at 50 Hz. Backscattered radiation from the atmosphere is collected with a 1 m diameter telescope and for aerosol measurements, the elastic backscatter at 355 nm and the nitrogen Raman scattering at 387 nm are accumulated. The ratio of the 355 nm and 387 nm signals is normalized in a region believed to be aerosol free, typically >30 km, to give the aerosol backscatter ratio. This method, utilizing the nitrogen Raman signal, eliminates the need for a reference density profile from another source, e.g., sonde or model, and provides a more accurate measure of the backscatter ratio.

2.2.6. Mauna Loa and Boulder (NOAA GMD)

[18] The NOAA/ESRL/Global Monitoring Division has been measuring aerosol backscatter with an Nd:YAG (532 nm, 1064 nm) lidar system since March 1994 at the MLO. MLO is located at 19.5°N, 155.6°W, 3.4 km above sea level on the north slope of the Mauna Loa volcano on the island of Hawaii and samples both tropical and midlatitude air depending on season and atmospheric circulation patterns.

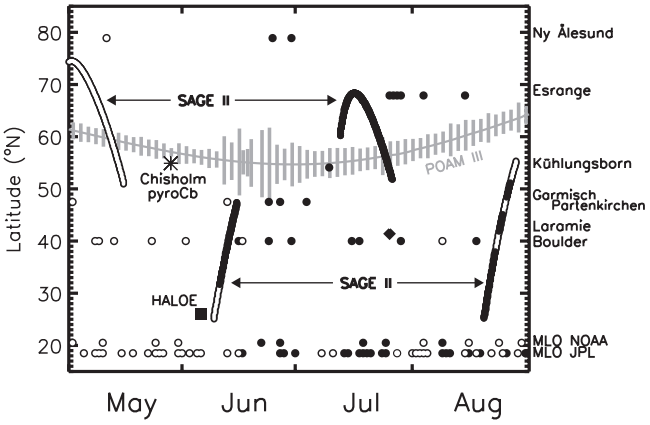

Figure 1. Location and date of the observations reported in this paper, expressed in time (abscissa) and latitude (ordinate). The Chisholm pyroCb is marked by an asterisk. POAM III data are represented as gray vertical bars straddling the POAM measurement latitude (gray line connecting the bars); bar length is proportional to stratospheric aerosol optical depth (see text for details). SAGE II symbols are circles, one per day, open for dates with no stratospheric aerosol layers and solid black if one or more layers are detected. Lidar symbols are circles, open for no-aerosol-layer and solid black for layer observations. HALOE symbol is a square. Laramie in situ symbol is a diamond. Lidar location names at approximate instrument latitude along the right axis (Mauna Loa lidars separated for clarity).

The lidar also measures water vapor and temperature. A smaller Nd:YAG (532 nm) aerosol system has been operated in Boulder, Colorado (40.0°N, 105.3°W, 1.6 km altitude) since August 1999. Both systems are operated weekly and are part of the NDACC.

2.3. In Situ Size Distributions

[19] In addition to the remote measurements there was one in situ profile measurement with a balloon-borne optical particle counter (OPC) which appears to have sampled the smoke. These OPCs have been flown regularly from Laramie, Wyoming (41°N, 105°W) since the early 1970s [*Hofmann et al.*, 1975; *Hofmann*, 1990; *Deshler et al.*, 2003]. The instrument initially developed by *Rosen* [1964] was modified in the early 1990s to increase the number of size bins and improve sensitivity [*Hofmann and Deshler*, 1991]. The instrument is presently capable of measuring particles between 0.15 and 2.0 μm in 12 radius ranges. Sizing errors are on the order of 10%. Concentration errors are dependent on the square root of the concentration, ranging from ~90 to 10% for concentrations ranging from 0.001 to 0.1 cm^{-3} [*Deshler et al.*, 2003]. Data from these measurements are publicly available through the World Wide Web (http://www-das.uwyo.edu/~deshler/).

2.4. Tropopause Height

[20] Tropopause-height data used herein come either from radiosonde reports or determined by the dynamical definition, that being the height of a prescribed potential vorticity (pv) surface. The most frequently chosen pv values for the midlatitude and high-latitude tropopause are between 1.5 and 2.0 pvu (potential vorticity units, 1 pvu = 10^{-6} K m^2 kg^{-1} s^{-1}; see [*Holton et al.*, 1995; *Beekmann et al.*, 1997]. We chose 3 pvu as a buffer to avoid troposphere overlap. For the tropopause height calculation we use the daily (1200 UTC) UK Met Office analyses [*Swinbank and O'Neill*, 1994] of temperature, wind, and geopotential height collocated both in time and space to the profile.

3. Results

[21] This paper synthesizes a large variety of measurement types, locations, and frequency on a seasonal timescale. Hence we introduce Figure 1, an overview of the measurement instruments, date, and latitude discussed in detail next. Figure 1 shows POAM III data as vertical bars whose length is scaled by stratospheric aerosol optical depth (details in section 3.1.2). All other instruments have individual symbols (see Figure 1 caption for details), which are filled in black if a stratospheric aerosol layer was measured. For SAGE II, a circle represents a full day of profiles; filled if any profiles had an aerosol layer.

[22] Figure 1 shows that this assemblage of instruments gives an effective seasonal sampling of the stratosphere from the Arctic to the tropics. Together they also offer a sampling frequency that permits an assessment of intraseasonal trends throughout much of this latitude range. The Chisholm latitude (54°N) and pyroCb date (28 May) are also indicated on Figure 1. It is apparent that there were no stratospheric aerosol enhancements in the month before the pyroCb, and many after. Next we present the details.

3.1. Satellite Solar Occultation (SO) Observations

3.1.1. Individual SO Profiles

[23] In this section we present four individual SO extinction profiles chosen to reveal important characteristics of the Chisholm pyroCb stratospheric plume. F08 determined that the Chisholm smoke plume the morning after the pyroCb, 29 May 2001, was an optically opaque cloud that reached 15 km, ~4–5 km above the local tropopause. *Rosenfeld et al.* [2007] showed that in the active convection the tops of the smoke-contaminated anvil were 1–2 km above the local temperature minimum (T_{min}), the top of the tropopause

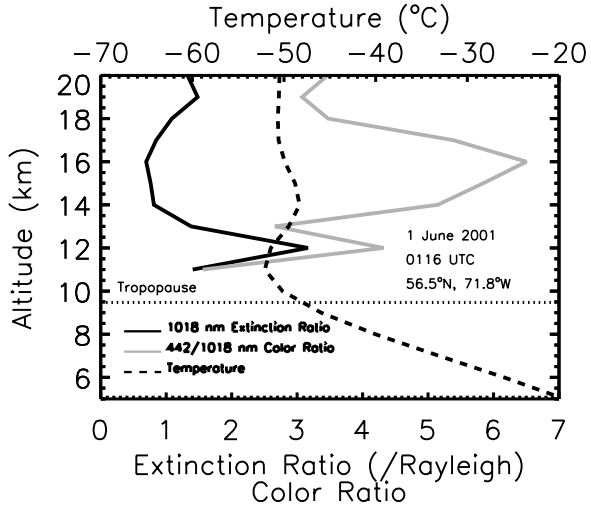

Figure 2. POAM III 1018 nm extinction ratio profile (black line) at 56.5°N, 71.8°W on 1 June 2001. POAM III color ratio (442 nm/1018 nm), gray line. Collocated temperature profile, black dashed line. Collocated tropopause height, horizontal dotted line.

region. Here we attempt to reconcile such values with the first two unambiguous stratospheric aerosol layers after 29 May, and a third layer observed 2 weeks after the pyroCb.

[24] On 1 June POAM III made a measurement over Quebec, shown in Figure 2. Figure 2 shows both the 1018 nm aerosol extinction ratio (normalized by Rayleigh extinction) and color ratio (the ratio of the 442 nm to 1018 nm extinctions). These are both shown in the context of the collocated temperature profile and tropopause altitude. The extinction ratio peaks at 12 km at three times Rayleigh, distinctly above background for that altitude. The tropopause is at roughly 9.5 km and the T_{min} is ~11 km. Thus this layer is unambiguously in the lowermost stratosphere (the potential temperature at 12 km was 355 K). The color ratio profile implies differences in particle size between the aerosol layer and the unperturbed altitudes above. In the limit, a particle population generally larger than 1018 nm would give no wavelength dependence, a color ratio of 1. We see that the color ratio decreases between the unenhanced altitudes and those with the aerosol layer. However, the color ratio even at the peak is considerably larger than one. Thus, the aerosol layer is composed of particles generally smaller than 1 μm. A nonnegligible wavelength dependence is found in the preponderance of the POAM and SAGE smoke layers.

[25] We used HYSPLIT [*Draxler and Hess*, 1998] to evaluate the source of this aerosol layer. Figure 3 shows a back trajectory started at the POAM layer at the measurement time of 0100 UTC. The trajectory passes over the Chisholm area at around the time of the pyroCb (~0200 UTC 29 May). Moreover it traces a path consistent with the early evolution of the Chisholm plume as described in F08. Hence we believe the POAM aerosol enhancement in Figure 2 is smoke from the Chisholm pyroCb.

[26] HALOE's measurement pattern in June 2001 began with sunset occultations on 5 June at about 30°N and subsequent southward progression such that by 8 June they passed 15°N and by 11 June passed south of the equator. In Figure 4 we see an enhancement of extinction on 5 June in HALOE's 2.45 μm channel in a profile over the subtropical Atlantic. This was the only sunset profile showing dramatically larger extinction in the lowermost stratosphere in early June. The layer of enhanced extinction extends from 1 to 4 km above the local tropopause. In this vicinity of the Atlantic (26°N, 45°W), F08 showed that the Chisholm plume was plainly evident in terms of the progression of the TOMS AI enhancements: the plume had initially passed north over north-central Canada, then south over Hudson Bay into the eastern United States by 1 June. In the 4 d thereafter part of the plume wound north toward Greenland and then southeast toward Europe while another portion moved into and apparently swirled in the area very close to the HALOE observation.

[27] Also in Figure 4 is a plot of color ratio using HALOE's 2.45 μm and 5.26 μm channels. Here we see color ratios much larger than 1 in the layer, peaking at nearly 4. The values of the 2.45 μm/5.26 μm color ratios of 3 to 4 from the HALOE measurements above the tropopause are incompatible with those of normal sulfuric acid stratospheric aerosols. Model calculations by *Hervig et al.* [1998] show that for typical background stratospheric aerosols the color ratio would be about 0.5 or less [see *Hervig et al.*, 1998, Figure 2], which is consistent with what is observed above the smoke layer. For typical volcanically enhanced aerosols the color ratio would be about 1.0 to 2.0. Even the maximum color ratio Hervig et al. find (2.5) for particle radii of about 1.2 μm, is still less than the measured values of 3 to 4. Hence we conclude that this substantial extinction enhancement with a unique HALOE color ratio is part of the Chisholm smoke plume.

[28] In the first week after injection the Chisholm pyroCb plume, according to F08, dispersed in such a way that the 14–15 daily Northern Hemisphere measurements from each SO instrument, separated by the typical 25° in longitude such as POAM's and HALOE's, had few opportunities to intercept. The two profiles discussed above were the best/earliest examples of an indisputable aerosol layer well above the tropopause in the first week after the pyroCb. There were no such stratospheric aerosol layers in POAM and HALOE earlier in 2001.

[29] By 11 June the daily frequency of stratospheric smoke layers as observed by SO instruments had begun increasing. On this date SAGE II (the June 2001 latitudinal measurement progression of which was such that it swept north to midlatitudes by 10 June) had four consecutive orbits of enhanced stratospheric aerosols over East Asia and the western Pacific, as seen on the map in Figure 5. Note also the positions of the POAM profile measurements and aerosol layer detections extending across most of Russia marked on the same map. The map is highly suggestive of a plume that was broadening both zonally and meridionally. Figure 6 displays a SAGE aerosol profile on 11 June with an extinction enhancement, greater than 40 times Rayleigh, in a layer well above the tropopause. This layer also exhibits strong wavelength dependence. Thus, like the POAM layer on 1 June, these particles have a characteristic radius less than 1 μm.

[30] Over the course of the northern spring/summer of 2001 there were over one hundred POAM, SAGE, and

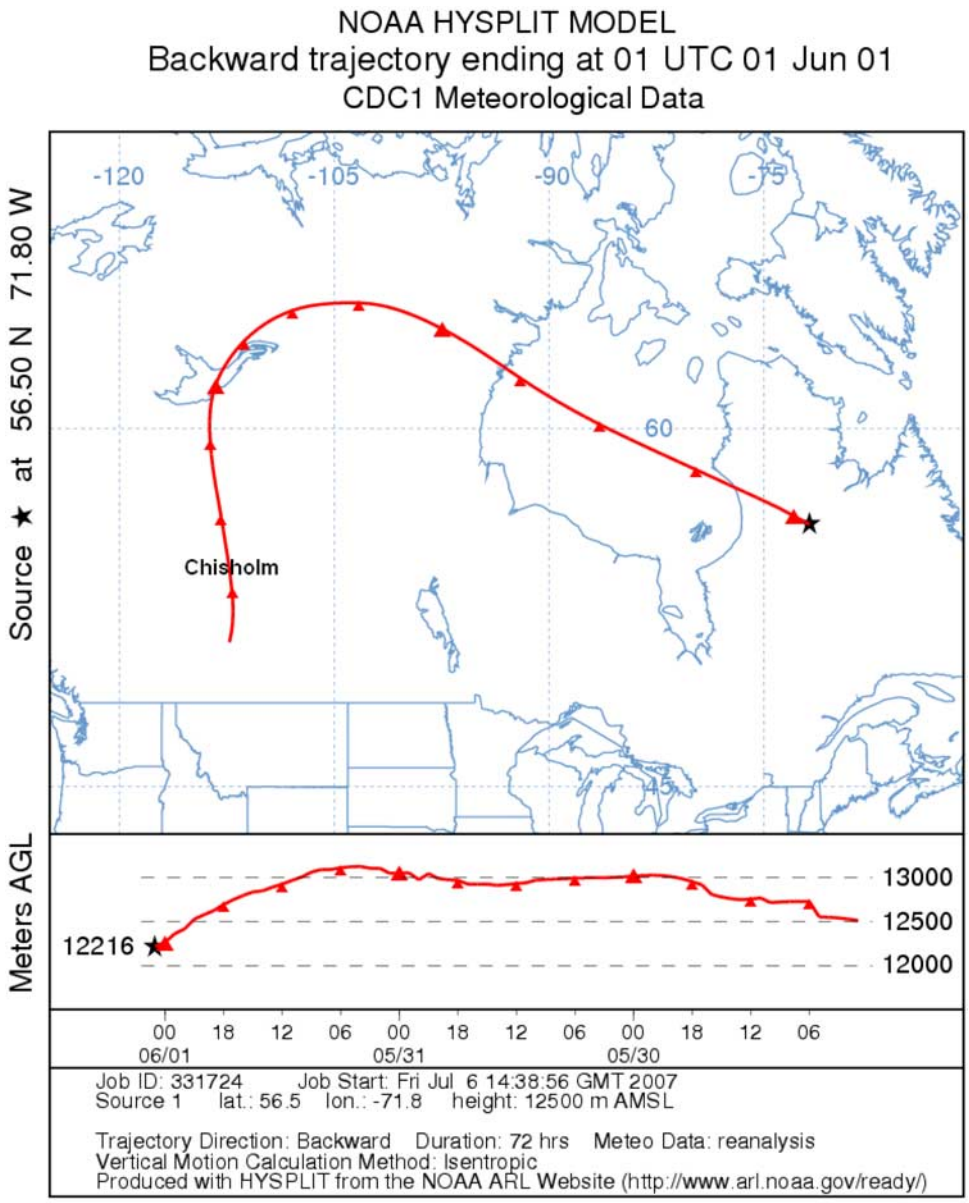

Figure 3. HYSPLIT backward trajectories initiated at the POAM III 1 June aerosol profile location (Figure 2). Length of trajectory is 72 h, roughly the time between the POAM measurement and the Chisholm pyroCb. Trajectory-start altitude is 12.5 km. PyroCb location is near the annotation "Chisholm."

HALOE profiles with lower stratospheric aerosol enhancements. One of the most remarkable of these is the POAM profile on 9 July at 54°N, 90°W shown in Figure 7. The aerosol layer's peak extinction was at an altitude of 18 km, approximately 9.5 km above the tropopause. This aerosol layer was one of four POAM aerosol layers observed at 17–18 km, all of which occurred in July. These represent the highest Chisholm smoke layers observed by the instruments discussed herein, and higher in potential temperature than any observed after the pyroCbs documented by *Fromm et al.* [2005, 2006]. It is outside the scope of this paper to analyze the Chisholm plume's smoke layer altitude; however, it is an important aspect of the pyroCb phenomenon that calls for future exploration.

3.1.2. Analysis of POAM, SAGE, and TOMS

[31] In the northern spring/summer of 2001 there were many POAM and SAGE profiles with stratospheric aerosol layers. The abundance of observations lends itself to statistical organization of these data.

[32] As mentioned in section 2.1, POAM made its measurements in a small latitude range (54° to 65°N). Every other day POAM made a full hemispheric complement (~14) of profiles. Because the vertical aerosol distribution was highly variable the 1018 nm extinction measurements are expressed in terms of lower stratospheric aerosol optical depth (AOD) by integrating between 30 km and the lowest altitude bin 2 km above the tropopause. A time series of the zonal average AOD from 1 May, before the Chisholm

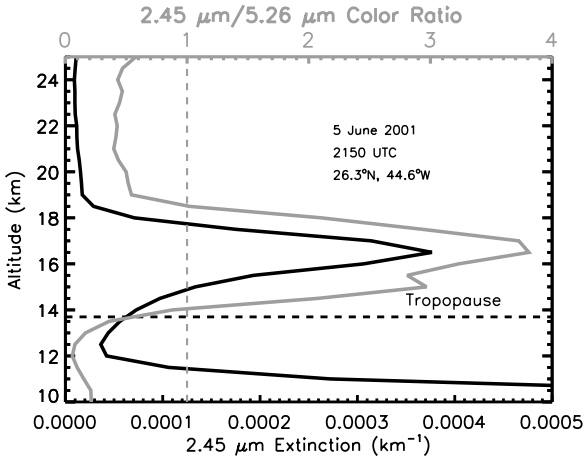

Figure 4. HALOE extinction profile at 26.3°N, 44.6°W on 5 June 2001. Black line is the 2.45 nm extinction. Gray line is the color ratio (2.45 nm/5.26 nm). Vertical gray dashed line at color ratio = 1 for reference. Collocated tropopause is shown by horizontal dashed line.

pyroCb, to the end of August is shown in Figure 8. The daily maximum TOMS AI within the hemispheric belt bounded by latitudes 45 and 75°N, encompassing the boreal forest zone, is also shown in Figure 8.

[33] The AI pattern in Figure 8 has one dominant feature, the large spike on 29 May, the day after the Chisholm pyroCb. The maximum AI on this day was the largest in the entire span of Nimbus VII and Earth Probe TOMS between 1979 and 2004. As discussed in F08 extreme AI such as this indicates strongly absorbing, elevated (i.e., UTLS) and optically dense plumes. The summer of 2001 contained no other AI plume nearly as extreme as that of 29 May. Figure 8 shows that in July and August the daily maximum AI did increase on several days to values well above the "background," for instance the double-digit AI plume on 25 August. Thus, there may have been other pyroconvective activity at those times, but between May and August 2001 the AI from the Chisholm pyroCb is over twice as large as any other. Thus the Chisholm pyroCb was (1) a singularly extreme event and (2) the only extreme smoke injection until at least late July or August.

[34] The POAM zonal average AOD before 29 May decreases slightly, reaching a minimum in late May. Soon after the pyroCb, AOD started increasing and by 23 June was roughly double the pre-pyroCb values. After 23 June the zonal average AOD declines somewhat, but is still greater at the end of the time series than prior to the Chisholm blowup. The doubling of the zonal average AOD is roughly equivalent to the AOD increase reported by *Fromm et al.* [2006] in the case of the Canberra Australia pyroCb, and roughly half of the AOD jump reported by *Fromm et al.* [2000, 2005] in the case of the Norman Wells (Northwest Territories) pyroCb of August 1998. These three cases are also those for which the TOMS AI plume peaked at the largest values in the TOMS record. Considering the AI pattern in Figure 8, the POAM AOD perturbation between June and August is most likely attributable exclusively to the Chisholm pyroCb.

[35] The inclined SAGE II orbit results in rapidly changing measurement latitudes relative to POAM. In the May-August 2001 time frame SAGE explored the mid and high northern latitudes in several discrete intervals, each lasting a few weeks. For this reason SAGE 1020 nm extinction ratio (total/Rayleigh) profiles are converted to a tropopause-relative altitude grid before computing range, mean, and median for those measurements north of 25°N. In Figure 9 the May time frame (before the Chisholm impact) is illustrated with the range shaded, and the median and mean overplotted. This unperturbed time frame is characterized

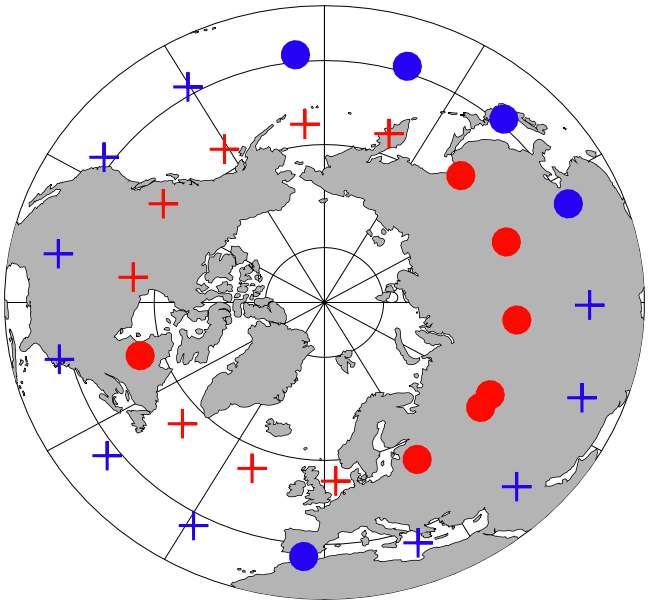

Figure 5. Polar map projection showing location of POAM III (red) and SAGE II (blue) measurements on 11 June 2001. Dots show where stratospheric aerosol enhancements were detected; plus signs identify unenhanced profiles.

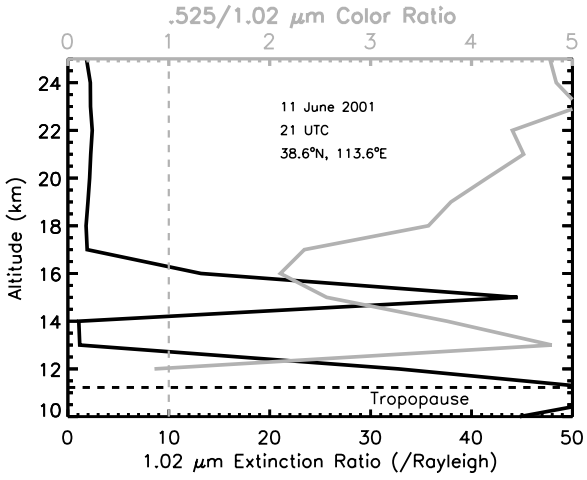

Figure 6. SAGE II 1020 nm extinction ratio profile (black line) at 38.6°N, 113.6°E on 11 June 2001. SAGE II color ratio (525 nm/1020 nm), gray line. Vertical gray dashed line at color ratio = 1 for reference. Collocated tropopause height, horizontal dotted line.

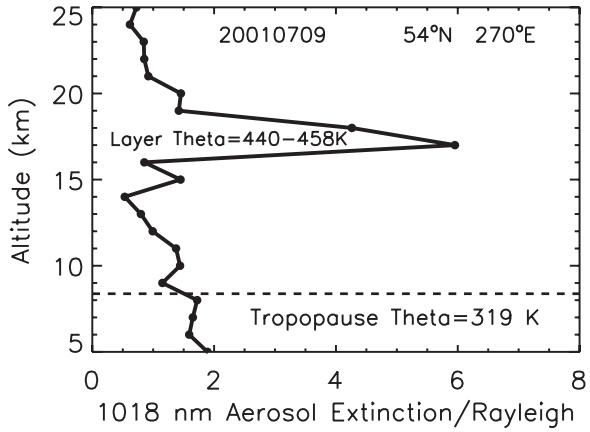

Figure 7. POAM III 1018 nm extinction ratio (1018 nm total extinction/Rayleigh) at 54.4°N, 90.0°W on 9 July 2001. Collocated tropopause is shown by horizontal dashed line.

by extinction ratio between about 1.8 at 3 km above the tropopause to 2.1 10 km above. In the entire vertical domain of Figure 9 the May mean and median are the same indicating the extinction ratio distribution is normal. In June the mean extinction ratio is larger than for May from bottom to top in Figure 9. From 7 to 10 km above the tropopause, the June mean and median are roughly equal; for lower altitudes, the mean departs considerably from the median (indicating a few extreme values) and ranges far outside the May maximum. In July the mean and median extinction ratio are nearly identical to May from 7 to 10 km above the tropopause. Below that the July mean and median diverge somewhat, but are both greater than the May maximum between 3 and 5 km above the tropopause. The August mean and median are roughly equal throughout the domain, mimicking the June values above 7 km above the tropopause. In the lower half, the August values appear to be relaxing back from the July values, but are still far larger than both May and June means.

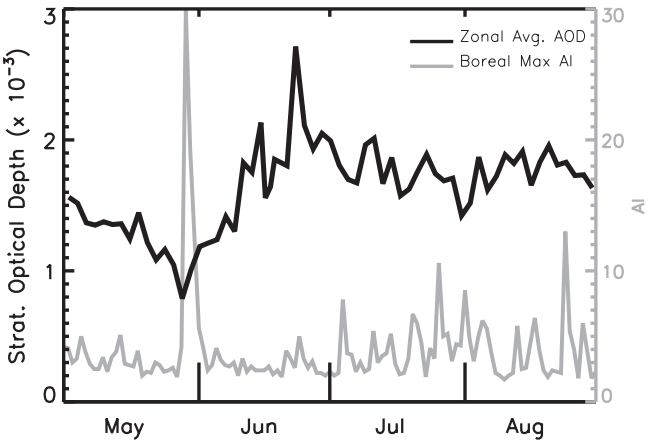

Figure 8. Daily/zonal average 1018 nm POAM III aerosol optical depth, May–August 2001, black line. Optical depth calculated by summing 1018 nm extinction from tropopause +2 km to 30 km. Gray line, daily maximum TOMS aerosol index north of 45°N.

[36] The SAGE variations in Figure 9 are a function of the specific latitude ranges sampled (see Figure 1) and the impact of the Chisholm smoke. Above 7 km with respect to the tropopause the extinction ratio distributions are exclusively normal. The shifts in these values from month to month are the result of variations in the sampling latitude. From 3 to 6 km above the tropopause the SAGE extinctions are strongly perturbed in June–August. The perturbation is spatially concentrated in June, indicated by the large mean-median difference. This decrease of this differential in July and August suggests that the enhanced aerosol burden is spread hemispherically.

3.2. Lidar Observations of the Chisholm Smoke

[37] In addition POAM, SAGE, and HALOE, seven ground-based lidars contributed measurements of the Chisholm plume. The lidar locations, wavelengths, and measurement dates are listed in Table 1. The subsections below are organized by instrument, in the order of decreasing latitude.

3.2.1. Ny Ålesund (79°N)

[38] Between May and August 2001 the lidar at Ny Ålesund was operated when meteorological conditions permitted. On 24 and 29 June anomalous stratospheric enhancements in backscatter and depolarization were recorded. In Figure 10 we show time-height curtain plots of backscatter coefficient and volume depolarization. The aerosol enhancements are manifested as small yet persistent increases in both backscatter and depolarization. On 24 June there is primarily a single aerosol layer between roughly 12.5 and 13 km altitude, 2 km above the tropopause, lasting the entire 10 h of measurements. On 29 June, the tropopause is at 9.5 km and above it are three aerosol layers. These layers are somewhat more highly backscattering and depolarizing than the 24 June layer. Two layers on 29 June, at about 12 and 13 km, persisted for the entire 12-h measurement span. A higher layer, at about 14 km (4.5 km above the tropopause) appears midway during the measurement time and lasted over 9 h. All of these backscattering layers on both dates exhibited depolarization, indicating a consistent

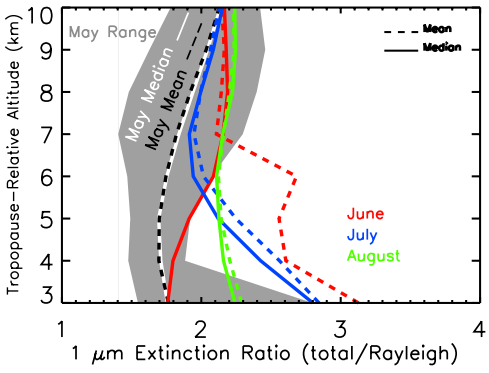

Figure 9. SAGE II 1 micron extinction ratio statistics for midlatitude spring/summer 2001 profiles. The bottom of this tropopause-relative ordinate is +3 km. May 2001 statistics include the range (shaded), median (white line), and average (black dashed line). Other months have only median (solid) and average (dashed). June (red), July (blue), and August (green).

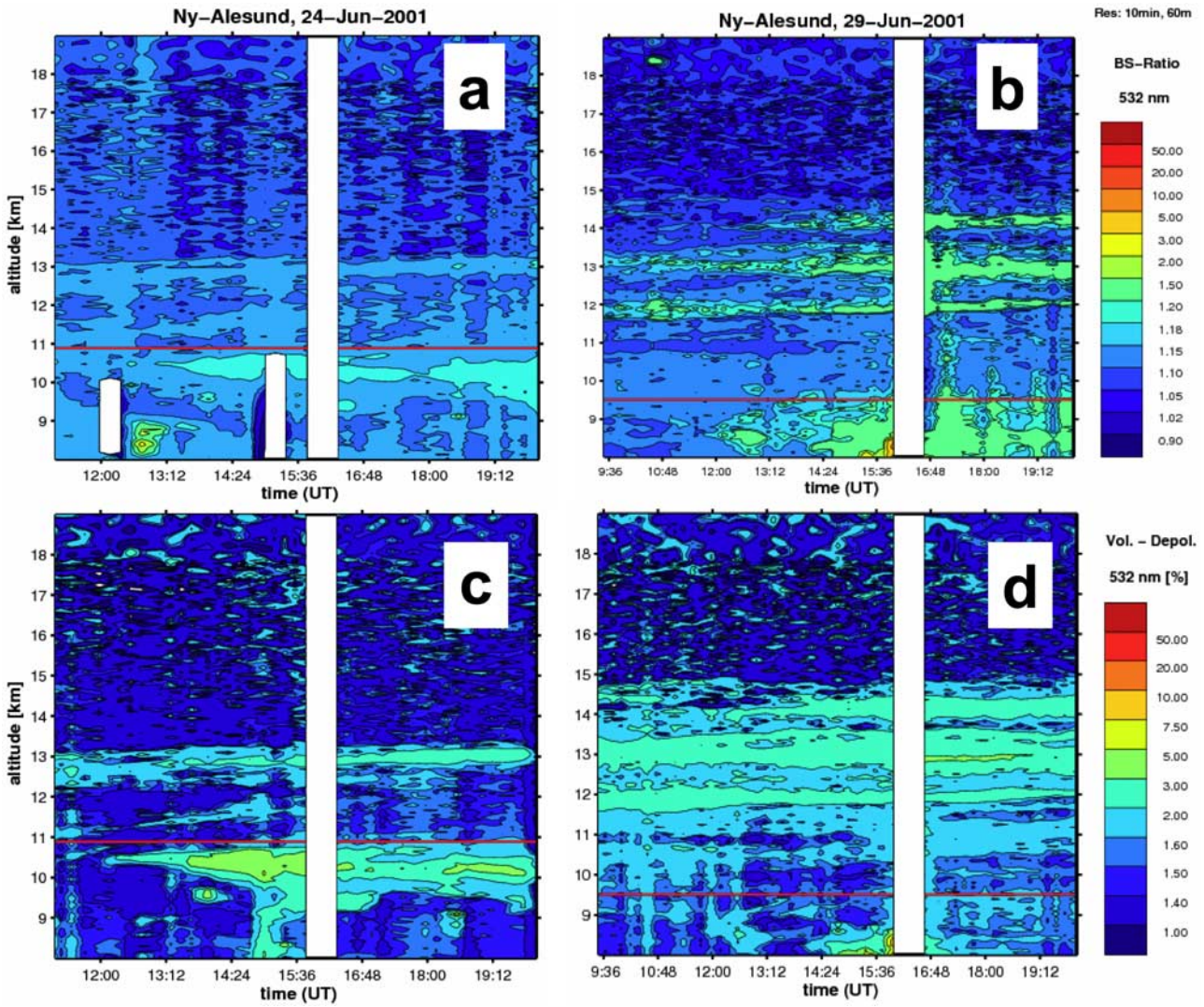

Figure 10. Ny Ålesund lidar time-height curtain of 532 nm (a and b) backscatter coefficient and (c and d) volume depolarization, in percent, for 24 June (Figures 10a and 10c) and 29 June (Figures 10b and 10d) 2001. Thin red line is the tropopause altitude.

composition of nonspherical (solid) particles. This same combination is what led *Siebert et al.* [2000] to conclude the existence of a smoke layer with solid particulates (possibly soot) over Scandinavia in July 1998. The persistence of these layers indicates that the aerosol enhancement is a large, quasi-continuous feature on both dates. The observations 5 d apart suggest that the aerosols being transported in the high Arctic 1 month after Chisholm were broad in horizontal scope. It was at this time (late June) that the POAM zonal average AOD reached its peak.

[39] In Figure 11 we display the depolarization data on each date as a single profile, and show an accompanying temperature profile from a radiosonde launched at the same location and time as the lidar measurement. There is a generally positive correlation between temperature and the aerosol abundance in the neighborhood of the layers. This correlation, which we characterize as a ''warm'' layer coincident with the aerosol enhancement may suggest that the solid aerosols are imbedded in a layer which has been radiatively modified by the aerosols. The temperature sounding is an independent measurement with high vertical resolution, but spatially separated by the drift of a balloon. Considering the deduced large horizontal extent of the persistent layers, it is likely that the radiosonde passed through the aerosol layer. Thus, although we have only two measurements of locally ''warm'' aerosol layers, we can state that (1) there is no inherent measurement contamination, (2) the lidar and radiosonde were likely sampling exactly the same air mass, and (3) an aged layer of absorbing aerosols such as smoke would reasonably have such a temperature impact.

[40] The aerosol feature on 29 June in Figure 11 is double peaked. The coincident radiosonde gives evidence of localized ''warming'' that matched remarkably well with the two distinct aerosol enhancements. The two local maxima in temperature at the altitudes of peak depolarization are indeed small; however, they are imbedded in a larger surrounding envelope of greater temperature with respect to the levels immediately above and below the two-layer aerosol enhancement.

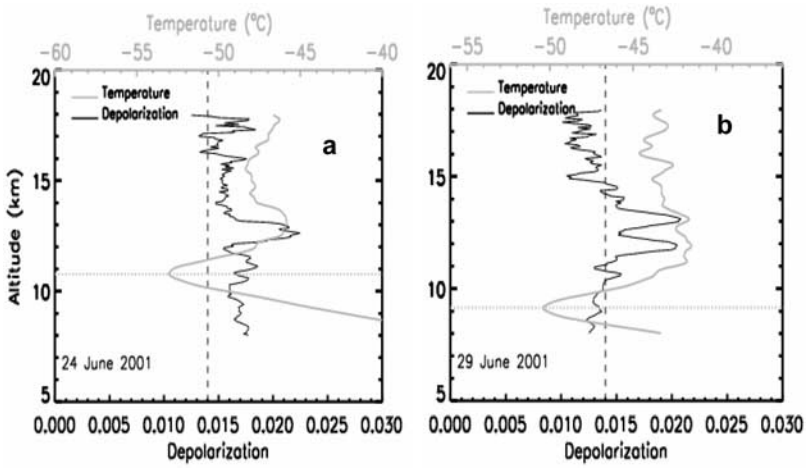

Figure 11. Depolarization profiles for a segment of the data shown in Figure 10. (a) For 24 June and (b) for 29 June. Black lines are the lidar data. Gray lines show radiosonde temperature (°C). Depolarization scale is at bottom; temperature scale is along the top. The vertical dashed line is a nominal background depolarization value. The gray horizontal line is the altitude of the temperature minimum.

3.2.2. Esrange (68°N)

[41] The Esrange lidar operated on six dates from 25 July to 14 August. Enhanced aerosols in the lower stratosphere, which might be smoke particles, were measured on each occasion (Figure 12). Figures 12a–12d reveal that aerosol enhancements were detected at Esrange on four consecutive days. This daily detection of enhanced stratospheric aerosols is suggestive of a quasi-continuous feature. Moreover, Figures 12e and 12f show that 1 week later, on 3 August and again on 14 August depolarizing layers were observed. Figure 8 indicates that in late July the zonal average lower stratospheric AOD (2 months after Chisholm) was still elevated with respect to pre-Chisholm. Thus, the POAM and Esrange lidar data are giving distinct yet consistent indications of a hemispheric aerosol perturbation.

[42] The depolarizing signal indicates solid aerosols, which makes them compatible with smoke and the observations made at Ny Ålesund. Below about 14 km altitude down to the tropopause aerosols are present on each is measurement day and show little fluctuation with altitude and a cross-polarized backscatter ratio of 1.5 to 2. On the first four measurement occasions, 25–28 July there are one or two narrow layers (600 m thick) in the altitude range 15 to 17 km. These "top layers" appear to be "cloud-like"; that is, they existed only for a few days, while the "bottom" layer from 14 km to the tropopause was present for 3 weeks as if the entire lowermost stratosphere was filled with solid particulates.

[43] Figure 12 also shows temperature profiles from the radiosonde location closest to the Esrange, at Bodø (67.2°N, 14.4°E, 279 km from Esrange). These temperature measurements are shown to support the tropopause determination, and to qualitatively show a thermal character of the air mass in which the aerosol layers were observed. We cannot draw similarly strong conclusions here as we did with Ny Ålesund because of the much greater radiosonde-lidar distance here and the variable time difference in measurements. However, the temperature profiles show that the aerosol enhancements are above the cold-point tropopause. Moreover, on 4 of the 6 dates shown, 25–27 July and 14 August there is some indication of locally warmer air in proximity to the aerosol layers.

3.2.3. Kühlungsborn (54°N)

[44] One quantitative measurement was made by the Kühlungsborn lidar in summer 2001, on 9 July (Figure 13). The profile shows little or no enhancement in backscatter in the unpolarized channel, but a substantial increase in the perpendicularly polarized channel. Here the enhancement occupies altitudes from above the local T_{min} (recorded by the Lindenberg radiosonde launched at 52°N, 14°E, 261 km from the lidar) to 16 km, 5 km above the T_{min}. The increase in cross-polarized backscatter indicates the presence of nonspherical particles. The accompanying temperature measurement, while not truly coincident, is close in both time and space to the lidar measurement. As with the Ny Ålesund observations, there is a correlation of the aerosol layer with an apparent "warm" layer that, together with the findings discussed earlier may be consistent with air radiatively impacted by absorbing smoke aerosols.

3.2.4. Garmisch-Partenkirchen (47°N)

[45] Lidar operation in spring 2001 was infrequent, and interrupted after 3 July for a field campaign. Four measurements were made in June and July 2001. The first one on 12 June (not shown) does not show any sign of a plume above the tropopause. Figure 14 shows observations on 23 and 26 June, and 3 July, of aerosol layers in the lowermost stratosphere at Garmisch-Partenkirchen. The tropopause level is taken from the Munich radiosonde which is launched about 100 km to the north at 0000 and 1200 UTC. On 23 June there is a sharp enhancement, approximately 2 km thick, with a backscattering peak 2 km above the tropopause (z = 13.8 km). On 26 June there is a multilayer enhancement 1–4 km above the tropopause (between 13 and 16 km). One week later, on 3 July, a relatively broad layer resides about 3 km above the tropopause (centered at 14.6 km), and the layer extends to 17 km.

[46] The temperature profiles reinforce the pattern in the layer observations from Ny Ålesund, Esrange, and Kühlungsborn –localized "warm" layers in proximity to the aerosol enhancements. Once again, we can only conclude

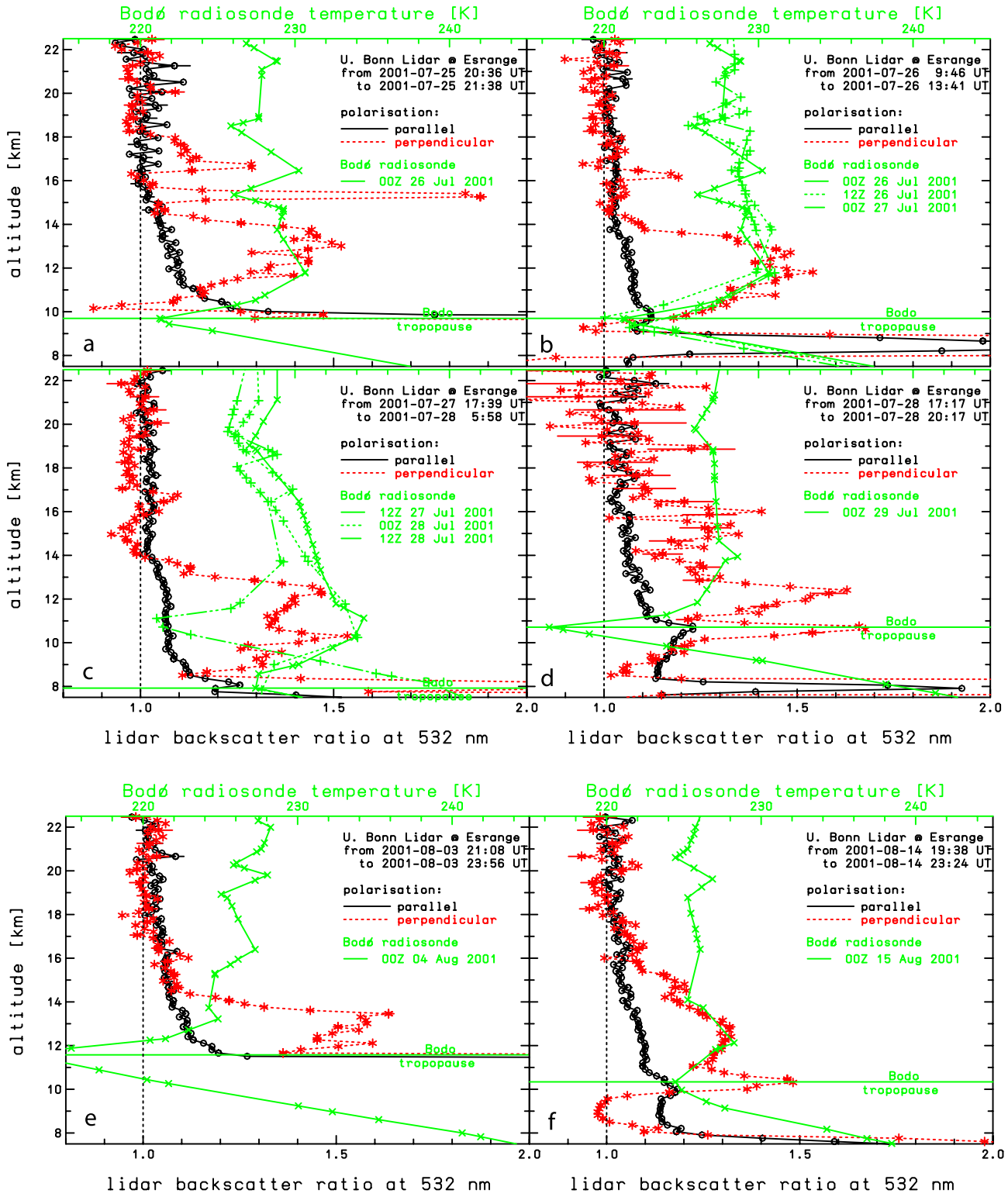

Figure 12. Lidar data from the Esrange. Six panels, one for each measurement date. (a–d) Four profiles from July 2001 and (e and f) two August 2001 profiles. Black line and symbols, parallel polarization 532 nm backscatter ratio. Red lines and symbols, perpendicular polarization backscatter ratio. Green line is radiosonde temperature (K) from Bodø, Norway (67.3°N, 14.7°E, ~279 km west of Esrange), at the measurement time closest to the lidar data. Temperature scale, along the top axis, color coded with the temperature plot.

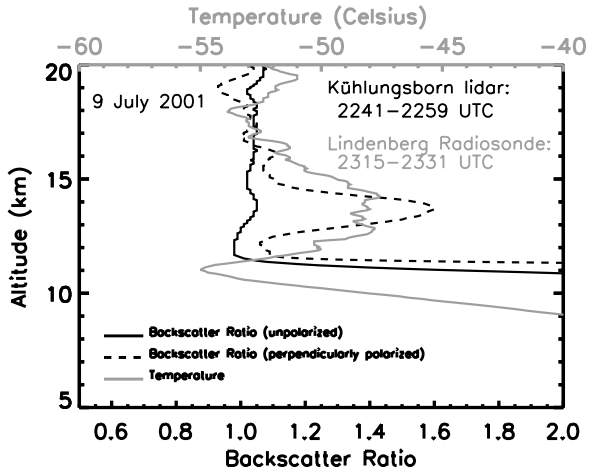

Figure 13. Lidar data from Kühlungsborn. Black solid line, backscatter ratio at 532 nm (unpolarized). Black dashed line, perpendicular polarization backscatter ratio. Gray line is radiosonde temperature (°C) from Lindenberg (52.2°N, 14.1°E, ∼261 km from Kühlungsborn) at the measurement time closest to the lidar data. Temperature scale along the top axis is gray shaded, as is the temperature plot.

that there is an apparent correlation, but the weight of the similar findings at four sites and ten occasions of aerosol layers provide sufficient motivation for a more systematic and exhaustive analysis of coincident smoke and UTLS temperature observations in future work.

[47] The 23 and 26 June measurements were made within 3 d of the two layer observations at Ny Ålesund. At this time POAM was recording its maximum zonal mean optical depth, at ∼54°N. Thus, it is evident that by this time the stratospheric Chisholm smoke was distributed around the hemisphere zonally and meridionally between at least 47–79°N.

3.2.5. Boulder (40°N)

[48] Measurements by the lidar in Boulder in 2001 were taken on 14 dates scattered between May and August (Table 1). Backscatter ratio profiles, on a tropopause-relative altitude grid, are shown in Figure 15. The tropopause height is from the standard WMO definition for Denver radiosondes (∼30 km south of Boulder) launched at ∼0000 UTC on measurement dates. For each month we color code the profile as a day-of-month scaling: violet on the rainbow scale for first, red for last. The four May profiles (Figure 15a) all appear similar, with gradual, monotonic increases from tropopause +10 km downward to tropopause +2 km, and a more rapid increase from there to the tropopause. There is no evidence in May of an aerosol layer above the tropopause. Stratospheric aerosol layers over Boulder began showing up sporadically in mid-June 2001. On 1 and 16 June (Figure 15b) two profiles have an appearance similar to the May profiles, but on 15, 23, and 29 June unambiguous aerosol enhancements are manifest. The 15 June profile has broad, multilayer backscatter enhancements from the tropopause to tropopause +4 km. On 23 June there are two distinct aerosol layers 1 and 3 km above the tropopause. The 29 June profile shows aerosol enhancements in a single, thick layer between 1 and 3 km above the tropopause.

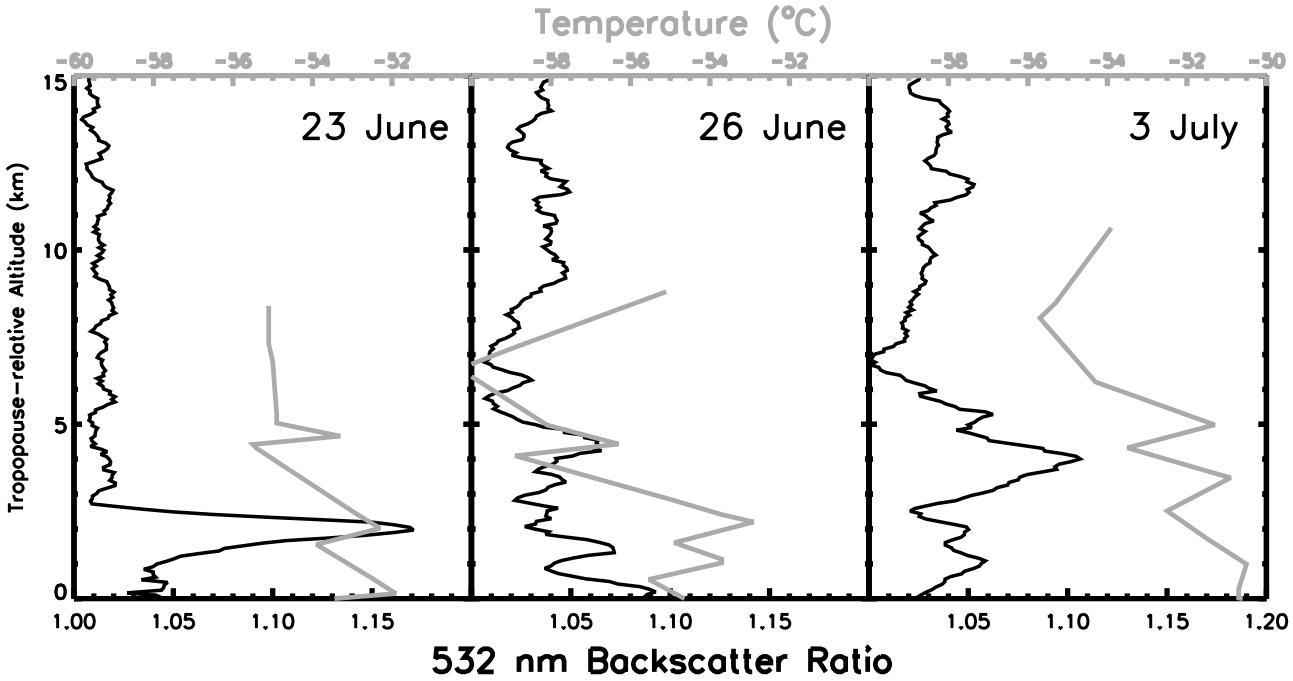

Figure 14. Three lidar profiles from Garmisch-Partenkirchen and radiosonde temperature profiles from Munch (∼90 km from the lidar). Vertical axis (in km) is a tropopause relative grid. Black line is parallel polarization 532 nm backscatter ratio; gray line is temperature (°C, scale on top and color coded to match plot). Panels are for 23 and 26 June and 3 July. Radiosonde measurement is from the 0000 UTC ascent closest to lidar measurement.

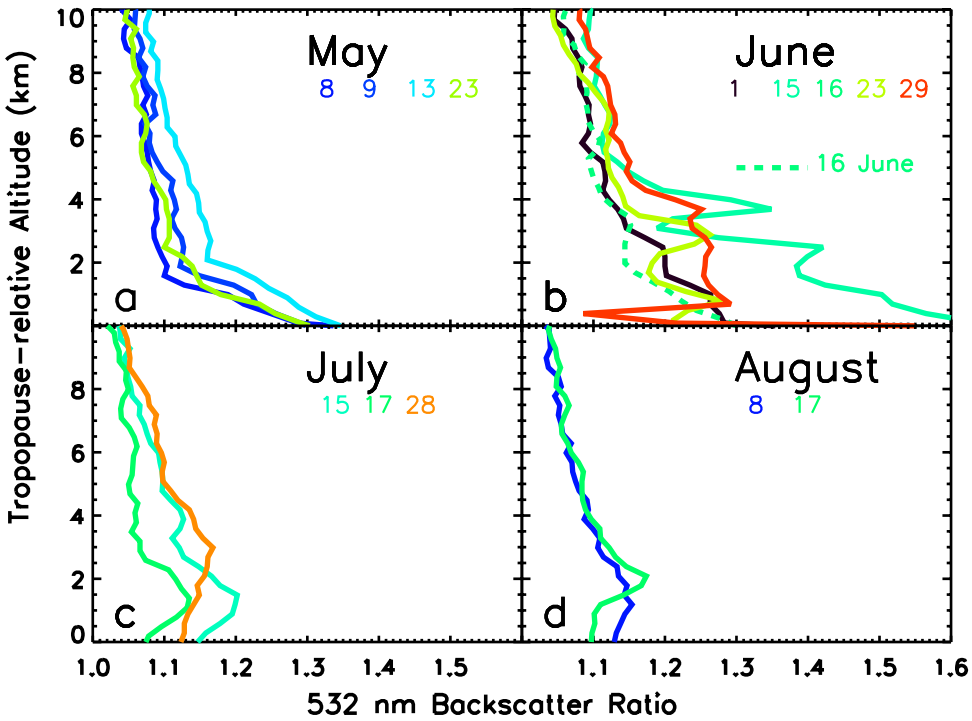

Figure 15. Lidar data from Boulder. (a) May, (b) June, (c) July, and (d) August. Backscatter ratio profiles at 532 nm are color coded to distinguish day of month. A rainbow color scale is used, violet for first day of month and red for last. Vertical axis (in km) is a tropopause relative grid. The profile in Figure 15b for 16 June is plotted as a dashed line to distinguish it from the 15 June plot.

[49] The 5 profiles in July and August (Figures 15c and 15d) each show local backscatter maxima 1–3 km above the tropopause. None of the backscatter ratios in the layer peak were as large as the layers observed in June. The Boulder observations in July and August are suggestive of a frequent but decaying aerosol layer just above the tropopause, a pattern similar to that observed at Esrange.

3.2.6. Mauna Loa (20°N)

[50] Two lidar systems operated at Mauna Loa. Because of differences in wavelength and ancillary data available, the measurements are displayed separately. Figure 16 (Figure 17) gives the JPL (NOAA GMD) lidar results. The profiles are color coded as for the Boulder measurements. The JPL lidar data files in the NDACC database include temperature and pressure, allowing the calculation of potential temperature (θ) for the vertical coordinate. θ in Figure 16 and altitude for the NOAA GMD data in Figure 17 give alternate perspectives on the height of layer features observed at essentially the same location. Between the two instruments there are 61 profiles between May and August 2001, enough to gain a qualitative sense of temporal changes in frequency of anomalous features. Figures 16 and 17 also show, in a single gray shade, all the profiles for May–August 2000, to give a basis with which to compare 2001 features.

[51] First we establish the baseline. In Figure 16 the gray profiles of May 2000 and the colored profiles of May 2001 show no enhancements in backscatter ratio between 350 and 500 K, which for Mauna Loa includes the tropical tropopause region and the stratosphere "overworld" [*Holton et al.*, 1995], the regime that anywhere on the globe is considered to be above the tropopause region. Although our understanding of the boundaries and transitions in the tropical troposphere/stratosphere interface is still being refined, there is no debate that $\theta > 400$ K is exclusively in the province of the stratosphere overworld. It is evident from the four panels of Figure 16 that there were no aerosol enhancements in 2000 at $\theta > 400$ K; furthermore, at $\theta < 380$ K, there were no enhancements in May, June, and August and at most only modest increases in two July profiles. We also evaluated the 1999 JPL lidar profiles (not shown) and found that, like 2000, there were no aerosol enhancements between May and August.

[52] The baseline picture of May 2000/2001 and June–August 2000 is in stark contrast to the observations in both instruments after May 2001. Figures 16b and 17b show that in June 2001, distinctive layer enhancements begin appearing in both the JPL and NOAA GMD measurements. The layers reside in the θ range 365–400 K and the height range 15.5–17.5 km. There were no NOAA GMD measurements in the first half of June, but there were five JPL lidar profiles between 2 and 15 June that exhibited no layers. From 16 to 30 June every NOAA GMD and JPL profile contains an aerosol layer in the lowermost stratosphere. Notably, there was an aerosol layer detected on 26 June (Figure 16b), the same day that the Garmisch-Partenkirchen lidar detected a stratospheric layer (and between observations at Ny Ålesund on 24 and 29 June). Thus, on or within a few days in late June 2001, anomalous aerosol in the lower stratosphere was spread from the tropics to the high Arctic.

[53] For July and August, Figures 16c and 16d have a smaller abscissa range than for Figures 16a and 16b: the layer enhancements trended to smaller peak values. The two

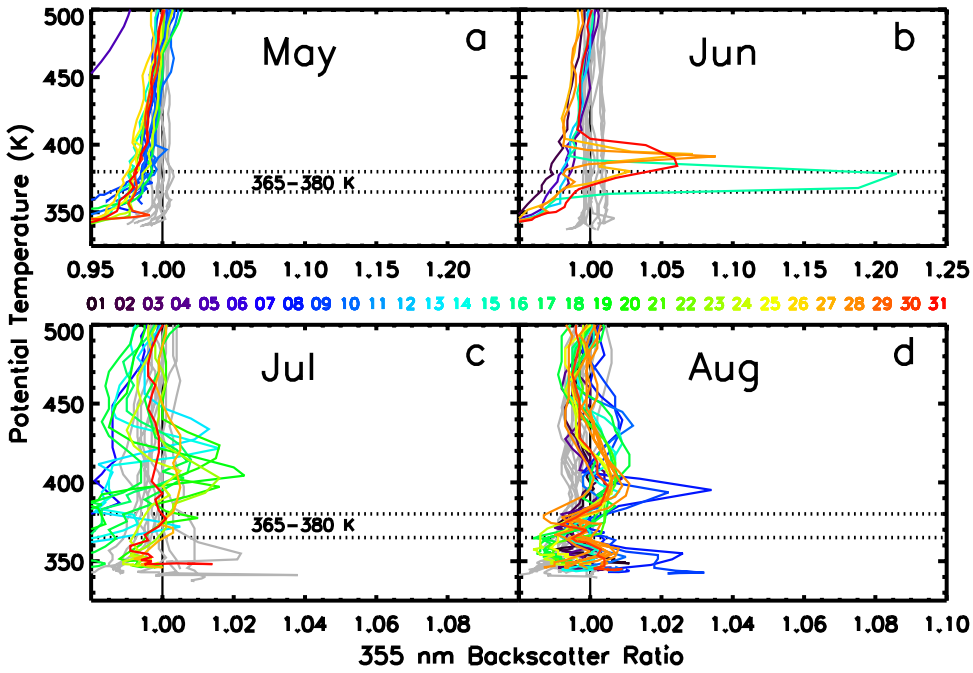

Figure 16. JPL lidar data from Mauna Loa. (a) May, (b) June, (c) July, and (d) August. Backscatter ratio profiles at 355 nm are color coded to distinguish day of month, using the rainbow color, violet for first day of month and red for last (see enumeration between top and bottom rows). Profiles for the same month of 2000 are plotted as gray lines. Vertical axis is potential temperature (K). Horizontal dashed lines at 365 and 380 K bracket the canonical lowermost stratosphere regime. Note the abscissa range for May and June is 0.9–1.25, whereas the July and August range is 0.95–1.10.

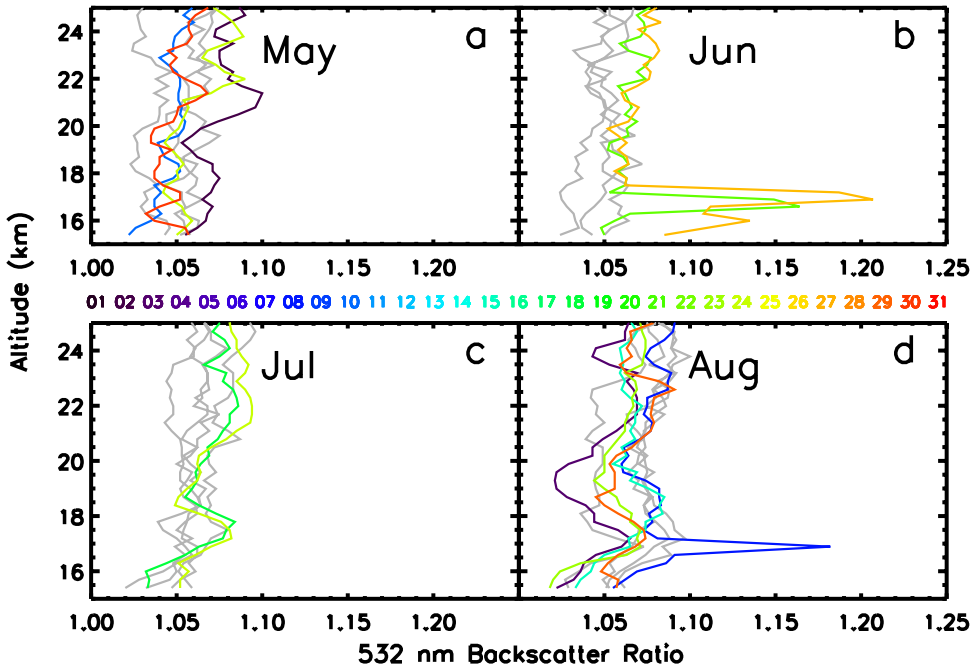

Figure 17. NOAA GMD lidar data from Mauna Loa. (a) May, (b) June, (c) July, and (d) August. Backscatter ratio profiles at 532 nm are color coded as described for Figure 16. Profiles for the same month of 2000 are plotted as gray lines. Vertical axis is altitude (km).

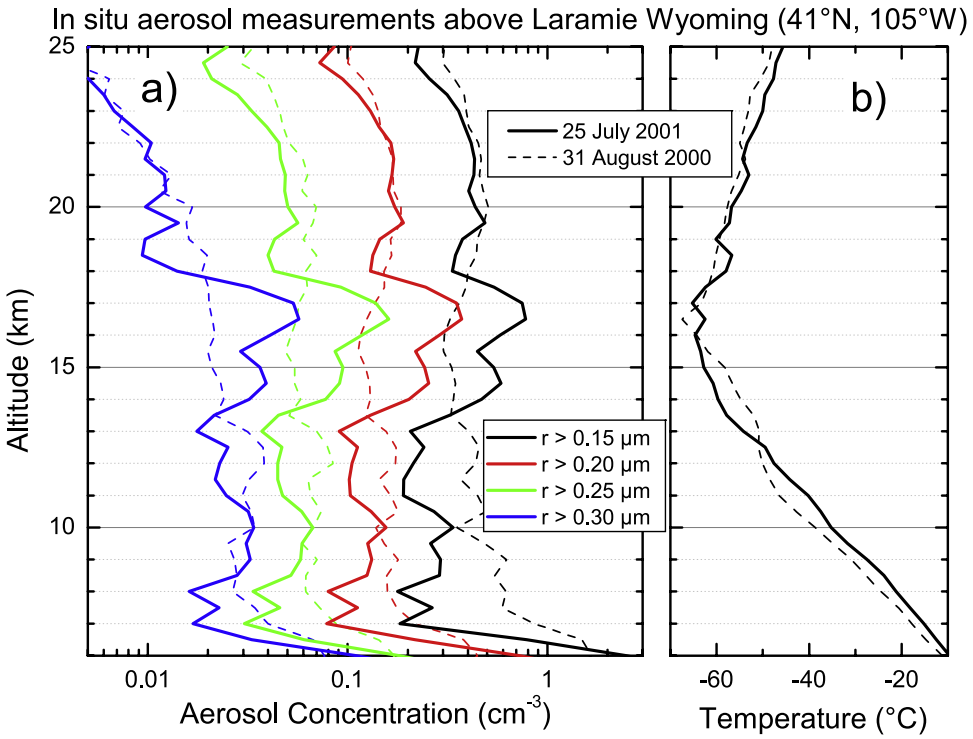

Figure 18. (a) Aerosol concentration profile at 4 sizes above Laramie, Wyoming, on 31 August 2000 (dashed lines) and 25 July 2001 (solid lines). (b) Temperature profiles on 31 August 2000 and 25 July 2001, indicating a tropopause between 14 and 15 km on the 2 d, respectively.

July 2001 NOAA GMD profiles (Figure 17c) have a small enhancement at about 17 km. The JPL lidar, with measurements between 7 and 31 July (Figure 16c), exhibited layers on the majority of measurement days, some extending to θ = 430 K.

[54] In early August both instruments captured a relatively sharp layer at about 400 K (JPL) and 17 km (NOAA GMD). At that same time the JPL profiles also exhibited a second, smoother layer peak at about 440–450 K. This peak does not appear in the NOAA GMD measurements. As in July, the August JPL lidar profiles are enhanced somewhere in the lower stratosphere on a large majority of the days of measurement. There appears to be a systematic decrease of top layer altitude (and to a lesser extent, strength as manifested by the peak backscatter) with day of month, from roughly 440 to 400 K.

[55] The two Mauna Loa lidars operated with sufficient frequency in the summers of 2000 and 2001 to conclude that there was a distinctive perturbation in the aerosol profile at this tropical location after the Chisholm pyroCb. The perturbation was first detected in mid-June, and was a dominant feature through August. The onset of this aerosol perturbation was about 2.5 weeks after the pyroCb. To determine if it is reasonable for the Chisholm plume to have arrived at Mauna Loa by in mid-June, we ran HYSPLIT forward trajectories (not shown) from the four SAGE II layers at 38°N shown in Figure 5, out to 16 June, when the first Mauna Loa layers were detected. Two of the four trajectories showed clearly that airflow from the SAGE point crossed the Mauna Loa latitude. Thus, we consider it reasonable that (1) the Chisholm plume in midlatitudes was transported into the tropical regime, (2) the arrival time at Mauna Loa is consistent with other layer profiles and the ambient meteorology, and (3) perhaps the Mauna Loa observations capture part of the leading edge of the Chisholm plume on its first sweep around the globe after the late-May injection.

3.3. In Situ Observations of the Chisholm Smoke at Laramie (41°N)

[56] In situ size-resolved aerosol concentration measurements above Laramie on 25 July 2001 may have also captured aerosol from the Chisholm pyroCb, after at least one circumnavigation. The aerosol appeared as concentration enhancements, by factors of 2 to 4, for aerosol between 0.15 and 0.30 μm radius at altitudes of 13 to 18 km (Figure 18). The concentration enhancements span the UTLS, peaking at 16.5 km (~1.5 km above the local tropopause) and extending 3 kilometers into the stratosphere. There is a hint of a concentration enhancement in a narrow layer at 17 km in the condensation nuclei profile (not shown), but no signature of the layer for particles >0.50 μm. The aerosol profiles on 25 July 2001 are shown compared with measurements on 31 August 2000, an unperturbed summer profile with a similar temperature profile, and tropopause ~14 km. In August 2000 the aerosol exhibit a typical profile for nonvolcanic UTLS aerosol, displaying a minimum in the UTLS, then increasing to a concentration maximum near 22 km, the well known stratospheric aerosol layer.

[57] For an indication of the aerosol enhancement carried in the Chisholm pyroCb plume the aerosol concentration measurements were fitted with bimodal lognormal size distributions [*Deshler et al.*, 2003] which were then used to calculate volume distributions for aerosol layers in and

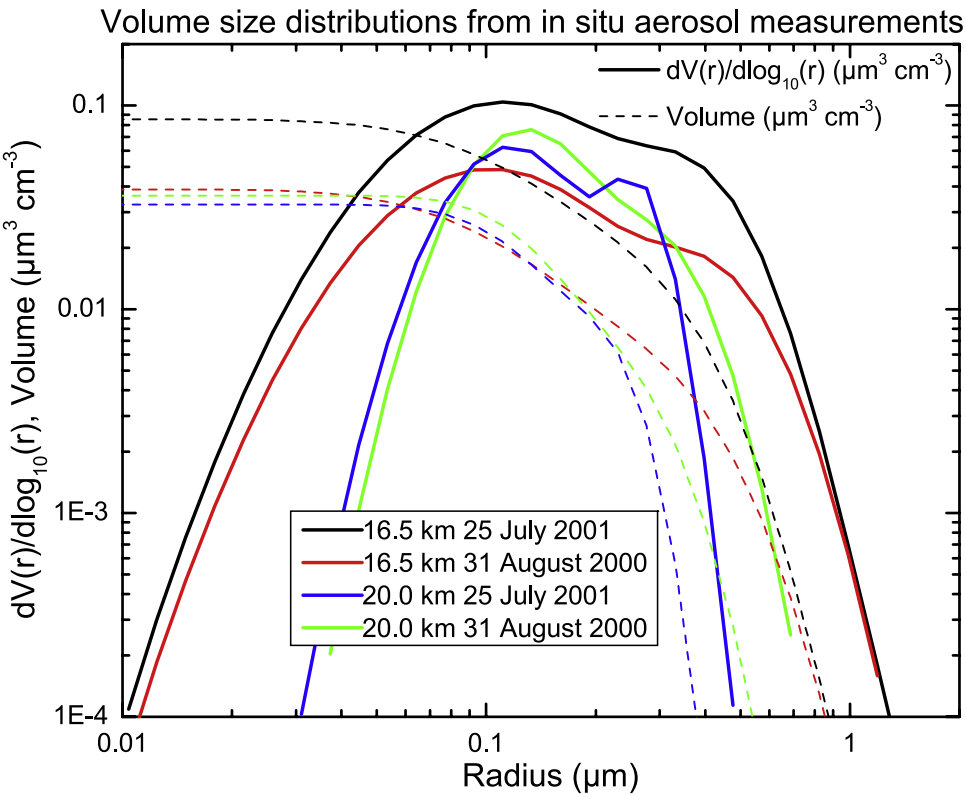

Figure 19. Differential and cumulative volume distributions from bimodal lognormal size distributions fit to the aerosol measurements at 16.5 and 20 km on 31 August 2000 (red and green) and 25 July 2001 (black and blue). The total volume carried in each layer is given by the point where the cumulative distribution lines intersect the left axis.

above the plume on 25 July 2001 and for similar altitudes on 31 August 2001. These are shown in Figure 19 as both differential and cumulative volume distributions. The distributions at 20 km on both days are quite similar and are narrower than the distributions at 16.5 km, as expected. The distributions at 16.5 km have approximately the same width, but the layer on 25 July 2001 shows a significant volume enhancement between 0.03 and 0.6 μm. The cumulative volume carried in the unperturbed layers on 31 August 2000 and at 20 km on 25 July 2001 were all similar, 0.3–0.4 μm^3 cm^{-3}, whereas the aerosol in the 16.5 km layer on 25 July 2001 had a volume of near 0.9 μm^3 cm^{-3}, a factor of 2 to 3 larger.

4. Summary and Conclusions

[58] This report complements the studies of the Chisholm (Alberta) pyroCb by FS03, *Rosenfeld et al.* [2007], and F08, who described the convective life cycle, injection of smoke into the UTLS, and the young stratospheric smoke plume. Here, we analyzed profiles measured by three solar occultation instruments (POAM III, SAGE II, and HALOE), seven ground based lidars, and a balloon-borne aerosol instrument. The satellite observations were between 25 and 69°N; the lidars are stationed between 20 and 79°N. Each instrument's peculiar measurement pattern in space and time was synthesized to develop a picture of the Chisholm plume's impressive spread into a hemispheric phenomenon.

[59] The Chisholm pyroCb on 28 May 2001 caused a spike in the TOMS AI that was the most intense AI plume in the more than 2-decade history of TOMS measurements. This stand-alone spike allowed us to conclude that the stratospheric aerosol perturbation reflected in the various profiles was smoke and that the Chisholm pyroCb was the singular cause.

[60] We used two SO profiles, from POAM III and HALOE, on 1 and 5 June respectively, to confirm and characterize the stratospheric impact of Chisholm within a week of the eruption. Back trajectories from the POAM layer matched the Chisholm blowup precisely; the HALOE profile (the first HALOE measurement identified as a stratospheric smoke layer) showed that the smoke plume reached subtropical latitudes in agreement with TOMS AI enhancements reported in the companion paper (F08).

[61] A second POAM profile, in July, showed the remarkable result that Chisholm smoke reached an altitude at least as high as 18 km, 458 K, 9.5 km above the tropopause. By 11 June 2001, 2 weeks after the pyroCb, the Chisholm plume was sufficiently broad that it was detected by several POAM and SAGE profiles. The "leading edge" at that time was over far eastern Asia and the northern Pacific Ocean at these two instruments' measurement latitudes.

[62] The stratospheric Chisholm smoke plume caused a doubling of the zonal average POAM AOD 4 weeks after the eruption, a gradual subsequent decay, yet still perturbed through August 2001. On or about 24 June (the time of the doubled AOD), aerosol layers were recorded at 79°, 54°,

47°, 40°, and 20°N: the plume ranged from the high Arctic to the northern tropics. SAGE data were presented in monthly statistical profiles to show that the plume persisted as high as 6 km above the tropopause, and spread from a regional phenomenon in June to hemispheric in July and August.

[63] In addition to the first-ever stratospheric smoke layer identified in HALOE data, this report also presented first-ever smoke signatures from ground-based lidar at Ny Ålesund, Esrange, Kühlungsborn, Garmisch-Partenkirchen, Boulder, and Mauna Loa.

[64] The Ny Ålesund measurements provided two new insights: (1) new constraint on north poleward transport of stratospheric pyroCb smoke and (2) a possible link between the smoke layer and localized increase in temperature. A similar (albeit qualitative) correlation between aerosol and temperature was observed at Esrange, Kühlungsborn, and Garmisch-Partenkirchen. This suggests an important forcing between the absorbing stratospheric smoke and diabatic heating. These preliminary findings call for a more exhaustive, systematic approach for future work.

[65] The lidar at Garmisch-Partenkirchen also measured Chisholm smoke layers on three dates in late June and early July. Lidar data from this location have been a cornerstone of stratospheric aerosol research dating back to 1976 [*Jäger*, 2005]. We are presently investigating the possibility that some episodes of enhanced aerosols in the lowermost stratosphere at this location, formerly characterized as volcanically forced, may have instead been caused by pyroCb.

[66] Perhaps the most surprising new insight gained from the many observations of the Chisholm smoke plume come from Mauna Loa. Two lidars, which recorded 61 profiles from May–August 2001, revealed a persistently perturbed aerosol condition at a location often influenced by tropical air masses. Our investigation showed that this perturbation did not occur in the prior two summers, that the altitude of many of the layers ruled out subvisual cirrus, and that the top-most impacted altitude was in close agreement with the POAM layer observation (at 55°N) at 458 K. These findings call for a deeper investigation into low-latitude profiles from both lidar and space-based instruments to assess the occurrence of tropical smoke layers, to distinguish UTLS smoke layers from subvisual cirrus, and to model stratospheric transport pathways between the midlatitudes and tropics.

[67] The Chisholm pyroCb was indeed a remarkable stratospheric pollution event. A single pyroconvective impulse, lasting on the order of 3 h, injected enough smoke into the UTLS to blanket the Northern Hemisphere from the tropics to the high Arctic, double the aerosol burden, and persist for at least 3 months. With the other pyroCbs reported in the literature, the Chisholm phenomenon signifies a recurring albeit episodic eruptive force akin to some minor volcanic eruptions. A preliminary indication discussed herein, that the smoke pall perturbed stratospheric temperature, is another aspect of the pyroCb that calls for more research.

[68] Some papers have reported a positive trend in the stratospheric aerosol load of the order of 1 to 10% per year for nonvolcanic periods [e.g., *Hofmann*, 1990]. However, *Deshler et al.* [2006] looked at a record that included three volcanic decay periods and concluded there was no long-term trend. *Bluth et al.* [1997] noted perturbations in the stratospheric aerosol optical depth between 1987 and 1991 that could not be reproduced by a volcanic eruption model. Perhaps these aerosol perturbations are a result of the pyroCb phenomenon. These questions deserve a closer look. The volumes of profile measurements made since the 1970s by satellite, lidar, and other instruments should be reexamined in light of the pyroCb discovery.

[69] At the time of this writing, space-based solar occultation views of the UTLS have become nearly nonexistent. SAGE III, POAM III, SAGE II, and HALOE measurements have all ceased. Stratospheric aerosol profiles are still being measured with instruments like Global Ozone Monitoring by Occultation of Stars (GOMOS) on Envisat [*Bertaux et al.*, 2000], Scanning Imaging Absorption Spectrometer for Atmospheric Chartography (SCIAMACHY) also on Envisat [*Bovensmann et al.*, 1999], and Cloud-Aerosol Lidar and Infrared Pathfinder Satellite Observations (CALIPSO) [*Winker et al.*, 2004]. However, monitoring stratospheric aerosol profiles into the indefinite future for important phenomena and new discoveries will likely fall more strongly on ground-based systems like those discussed herein. We consider it important to call for increased coverage of lidars, coordination among the measurement teams, and strategies for optimizing frequency/consistency of operation to probe the important UTLS.

[70] **Acknowledgments.** M.G. acknowledges the provision of Lindenberg radiosonde data by the German Weather Service (DWD). We thank N. Spichtinger-Rakowsky for her modeling effort. Some of the lidar data used in this publication were obtained from the database maintained by the Network for the Detection of Atmospheric Composition Change (NDACC) and are publicly available (see http://www.ndacc.org). The balloon-borne measurements were completed with support from the U.S. National Science Foundation (grant ATM 0437406) and are publicly available (http://www-das.uwyo.edu/~deshler/). M.D.F. and E.P.S. were supported in part by a grant from the NASA Office of Earth Science and in part by NRL internal funding (from the Office of Naval Research).

References

Alfred, J., M. Fromm, R. Bevilacqua, G. Nedoluha, A. Strawa, L. Poole, and J. Wickert (2007), Observations and analysis of polar stratospheric clouds detected by POAM III and SAGE III during the SOLVE II/VINTERSOL campaign in the 2002/2003 Northern Hemisphere winter, *Atmos. Chem. Phys.*, *7*, 2151–2163.

Alpers, M., R. Eixmann, J. Höffner, T. Köpnick, J. Schneider, and U. von Zahn (1999), The Rayleigh/Mie/Raman lidar at IAP Kühlungsborn, *J. Aerosol. Sci.*, *30*, Suppl. 1, S637–S638.

Alpers, M., M. Gerding, J. Höffner, and U. von Zahn (2000), NLC particle properties from a five-color lidar observation at 54°N, *J. Geophys. Res.*, *105*(D10), 12,235–12,240.

Alpers, M., R. Eixmann, C. Fricke-Begemann, M. Gerding, and J. Höffner (2004), Temperature lidar measurements from 1 to 105 km altitude using resonance, Rayleigh, and Rotational Raman scattering, *Atmos. Chem. Phys.*, *4*, 793–800.

Beekmann, M., et al. (1997), Regional and global tropopause fold occurrence and related ozone flux across the tropopause, *J. Atmos. Chem.*, *28*, 29–44.

Bertaux, J.-L., E. Kyrölä, and T. Wehr (2000), Stellar occultation technique for atmospheric ozone monitoring: GOMOS on Envisat, *Earth Obs. Q.*, *67*, 17–20.

Bevilacqua, R. M., et al. (2002), Observations and analysis of PSCs detected by POAM III during the 1999/2000 Northern Hemisphere winter, *J. Geophys. Res.*, *107*(D20), 8281, doi:10.1029/2001JD000477.

Blum, U., and K. H. Fricke (2005), The Bonn University lidar at the Esrange: Technical description and capabilities for atmospheric research, *Ann. Geophys.*, *23*, 1645–1658, sref:1432-0576/ag/2005-23-1645.

Bluth, G., W. Rose, I. Sprod, and A. Krueger (1997), Stratospheric loading of sulfur from explosive volcanic eruptions, *J. Geol.*, *105*, 671–683.

Bovensmann, H., J. Burrows, M. Buchwitz, J. Frerick, S. Noël, V. Rozanov, K. Chance, and A. Goede (1999), SCIAMACHY: Mission objectives and measurement modes, *J. Atmos. Sci.*, *56*(2), 127–150.

Brasseur, G., and S. Solomon (1986), *Aeronomy of the Middle Atmosphere*, 452 pp., D. Reidel, Dordrecht, Netherlands.

Crutzen, P., and J. Birks (1982), The atmosphere after a nuclear war: twilight at noon, *Ambio*, *11*, 114–125.

Daerden, F., N. Larsen, S. Chabrillat, Q. Errera, S. Bonjean, D. Fonteyn, K. Hoppel, and M. Fromm (2007), A 3D-CTM with detailed online PSC-microphysics: Analysis of the Antarctic winter 2003 by comparison with satellite observations, *Atmos. Chem. Phys.*, *7*, 1755–1772.

Deshler, T., M. E. Hervig, D. J. Hofmann, J. M. Rosen, and J. B. Liley (2003), Thirty years of in situ stratospheric aerosol size distribution measurements from Laramie, Wyoming (41°N), using balloon-borne instruments, *J. Geophys. Res.*, *108*(D5), 4167, doi:10.1029/2002JD002514.

Deshler, T., R. Anderson-Sprecher, H. Jäger, J. Barnes, D. J. Hofmann, B. Clemesha, D. Simonich, R. G. Grainger, and S. Godin-Beekmann (2006), Trends in the non-volcanic component of stratospheric aerosol over the period 1971–2004, *J. Geophys. Res.*, *111*, D01201, doi:10.1029/2005JD006089.

Draxler, R., and G. Hess (1998), An overview of the HYSPLIT-4 modelling system for trajectories, dispersion, and deposition, *Aust. Meteorol. Mag.*, *47*, 295–308.

Freudenthaler, V., F. Homburg, and H. Jäger (1994), Ground-based mobile scanning lidar for remote sensing of contrails, *Ann. Geophys.*, *12*, 956–961.

Fromm, M., and R. Servranckx (2003), Transport of forest fire smoke, above the tropopause, supercell convection, *Geophys. Res. Lett.*, *30*(10), 1542, doi:10.1029/2002GL016820.

Fromm, M., J. Alfred, K. Hoppel, J. Hornstein, R. Bevilacqua, E. Shettle, R. Servranckx, Z. Li, and B. Stocks (2000), Observations of boreal forest fire smoke in the stratosphere by POAM III, SAGE II, and lidar in 1998, *Geophys. Res. Lett.*, *27*, 1407–1410.

Fromm, M., J. Alfred, and M. Pitts (2003), A unified, long-term, high-latitude stratospheric aerosol and cloud database using SAM II, SAGE II, and POAM II/III data: Algorithm description, database definition, and climatology, *J. Geophys. Res.*, *108*(D12), 4366, doi:10.1029/2002JD002772.

Fromm, M., R. Bevilacqua, B. Stocks, and R. Servranckx (2004), New directions: Eruptive transport to the stratosphere: Add fire-convection to volcanoes, *Atmos. Environ.*, *38*, 163–165.

Fromm, M., R. Bevilacqua, R. Servranckx, J. Rosen, J. Thayer, J. Herman, D. Larko, and R. Servranckx (2005), Pyro-cumulonimbus injection of smoke to the stratosphere: Observations and impact of a super blowup in northwestern Canada on 3–4 August 1998, *J. Geophys. Res.*, *110*, D08205, doi:10.1029/2004JD005350.

Fromm, M., A. Tupper, D. Rosenfeld, R. Servranckx, and R. McRae (2006), Violent pyro-convective storm devastates Australia's capital and pollutes the stratosphere, *Geophys. Res. Lett.*, *33*, L05815, doi:10.1029/2005GL025161.

Fromm, M., O. Torres, D. Diner, D. Lindsey, B. Vant Hull, R. Servranckx, E. P. Shettle, and Z. Li (2008), Stratospheric impact of the Chisholm pyrocumulonimbus eruption: 1. Earth-viewing satellite perspective, *J. Geophys. Res.*, doi:10.1029/2007JD009153, in press.

Hervig, M. E. (1999), Stratospheric clouds over England, *Geophys. Res. Lett.*, *26*, 1137–1140.

Hervig, M., and M. McHugh (1999), Cirrus detection using HALOE measurements, *Geophys. Res. Lett.*, *26*, 719–722.

Hervig, M. E., T. Deshler, and J. M. Russell (1998), Aerosol size distributions obtained from HALOE spectral extinction measurements, *J. Geophys. Res.*, *103*, 1573–1583.

Hofmann, D. (1990), Increase in the stratospheric background sulfuric-acid aerosol mass in the past 10 years, *Science*, *248*(4958), 996–1000.

Hofmann, D. J., and T. Deshler (1991), Stratospheric cloud observations during formation of the Antarctic ozone hole in 1989, *J. Geophys. Res.*, *96*, 2897–2912.

Hofmann, D. J., J. M. Rosen, T. J. Pepin, and R. G. Pinnick (1975), Stratospheric aerosol measurements I: Time variations at northern midlatitudes, *J. Atmos. Sci.*, *32*, 1446–1456.

Holton, J., P. Haynes, M. McIntyre, A. Douglas, R. Rood, and L. Pfister (1995), Stratosphere-troposphere exchange, *Rev. Geophys.*, *33*, 403–439.

Jäger, H. (2005), Long-term record of lidar observations of the stratospheric aerosol layer at Garmisch-Partenkirchen, *J. Geophys. Res.*, *110*, D08106, doi:10.1029/2004JD005506.

Jost, H.-J., et al. (2004), In-situ observations of mid-latitude forest fire plumes deep in the stratosphere, *Geophys. Res. Lett.*, *31*, L11101, doi:10.1029/2003GL019253.

Klett, J. D. (1985), Lidar inversions with variable backscatter/extinction ratios, *Appl. Opt.*, *24*, 1638–1643.

Labitzke, K., and M. P. McCormick (1992), Stratospheric temperature increases due to Pinatubo aerosols, *Geophys. Res. Lett.*, *19*(2), 207–210.

Livesey, N., M. Fromm, J. Waters, G. Manney, M. Santee, and W. Read (2004), Enhancements in lower stratospheric CH_3CN observed by UARS MLS following boreal forest fires, *J. Geophys. Res.*, *109*, D06308, doi:10.1029/2003JD004055.

Lucke, R. L., et al. (1999), The Polar Ozone and Aerosol Measurement (POAM III) instrument and early validation results, *J. Geophys. Res.*, *104*, 18,785–18,799.

Mauldin, L. E., III, N. H. Zaun, M. P. McCormick, J. H. Guy, and W. Vaughn (1985), Stratospheric Aerosol and Gas Experiment II instrument: A functional description, *Opt. Eng.*, *24*, 307–312.

Palm, S. P., M. Fromm, and J. Spinhirne (2005), Observations of Antarctic polar stratospheric clouds by the Geoscience Laser Altimeter System (GLAS), *Geophys. Res. Lett.*, *32*, L22S04, doi:10.1029/2005GL023524.

Poulida, O., R. Dickerson, and A. Heymsfield (1996), Stratosphere-troposphere exchange in a midlatitude mesoscale convective complex: 1. Observations, *J. Geophys. Res.*, *101*(D3), 6823–6836.

Pyne, S., and P. Omi (1986), Wildland fires and nuclear winters: Selected reconstruction of historical large fires, *Rep. DNA-TR-85-396*, 167 pp., Def. Doc. Cent., Alexandria, Va., Feb.

Randall, C. E., R. M. Bevilacqua, J. D. Lumpe, and K. W. Hoppel (2001), Validation of POAM III Aerosols: Comparison to SAGE II and HALOE, *J. Geophys. Res.*, *106*, 27,525–27,536.

Rauthe, M., M. Gerding, J. Höffner, and F.-J. Lübken (2006), Lidar temperature measurements of gravity waves over Kühlungsborn (54°N) from 1 to 105 km: A winter-summer comparison, *J. Geophys. Res.*, *111*, D24108, doi:10.1029/2006JD007354.

Reber, C. A., C. E. Trevathan, R. J. McNeal, and M. R. Luther (1993), The Upper Atmosphere Research Satellite (UARS) mission, *J. Geophys. Res.*, *98*, 10,643–10,647.

Ritter, C., A. Kische, and R. Neuber (2004), Tropospheric aerosol characterized by a Raman lidar over Spitsbergen, in *22nd International Laser Radar Conference (ILRC 2004): 12–16 July 2004, Matera, Italy*, edited by G. Pappalardo and A. Amodeo, *Eur. Space Agency Spec. Publ., ESA-SP 561*, 459–462.

Rizi, V., F. Masci, G. Redaelli, P. Di Carlo, M. Iarlori, G. Visconti, and L. Thomason (2000), Lidar and SAGE II observations of Shishaldin volcano aerosols and lower stratospheric transport, *Geophys. Res. Lett.*, *27*, 3445–3448.

Rose, W., et al. (2003), The February–March 2000 eruption of Hekla, Iceland from a satellite perspective, in *Volcanism and the Earth's Atmosphere*, *Geophys. Monogr. Ser.*, vol. 139, edited by A. Robock and C. Oppenheimer, pp. 107–132, AGU, Washington, D. C.

Rosen, J. M. (1964), The vertical distribution of dust to 30 km, *J. Geophys. Res.*, *69*, 4673–4676.

Rosenfeld, D., M. Fromm, J. Trentmann, G. Luderer, M. Andreae, and R. Servranckx (2007), The Chisholm firestorm: Observed microstructure, precipitation and lightning activity of a pyro-Cb, *Atmos. Chem. Phys.*, *7*, 645–659.

Russell, J. M., III, L. Gordley, J. Park, S. Drayson, W. Hesketh, R. Cicerone, A. Tuck, J. Frederick, J. Harries, and P. Crutzen (1993), The Halogen Occultation Experiment, *J. Geophys. Res.*, *98*, 10,777–10,797.

Russell, P., et al. (2005), Aerosol optical depth measurements by airborne Sun photometer in SOLVE II: Comparisons to SAGE III, POAM III and airborne spectrometer measurements, *Atmos. Chem. Phys.*, *5*, 1311–1339.

Schneider, J., and R. Eixmann (2002), Three years of routine Raman lidar measurements of tropospheric aerosols: Backscattering, extinction, and residual layer height, *Atmos. Chem. Phys.*, *2*, 313–323.

Siebert, J., C. Timmis, G. Vaughan, and K. Fricke (2000), A strange cloud in the Arctic summer stratosphere 1998 above Esrange (68°N), Sweden, *Ann. Geophys.*, *18*, 505–509.

Sigurdsson, H., B. Houghton, S. McNutt, H. Rymer, and J. Stix (2000), *Encyclopaedia of Volcanoes*, 1417 pp., Elsevier, New York.

Stocks, B., and D. McRae (1991), The Canada/United States cooperative mass fire behavior and atmospheric environmental impact study, paper presented at Eleventh Conference on Fire and Forest Meteorology, Soc. of Am. For., Bethesda, Md., 16–19 Apr.

Swinbank, R., and A. O'Neill (1994), A stratosphere-troposphere data assimilation system, *Mon. Weather Rev.*, *122*, 602–686.

Thomason, L., L. Poole, and T. Deshler (1997), A global climatology of stratospheric aerosol surface area density as deduced from SAGE II: 1984–1994, *J. Geophys. Res.*, *102*, 8967–8976.

Turco, R., O. Toon, T. Ackerman, J. Pollack, and C. Sagan (1983), Nuclear winter: Global consequences of multiple nuclear explosions, *Science*, *222*, 1283–1292.

Waibel, A., H. Fischer, F. Wienhold, P. Siegmund, B. Lee, J. Ström, J. Lelieveld, and P. Crutzen (1999), Highly elevated carbon monoxide concentrations in the upper troposphere and lowermost stratosphere at northern midlatitudes during the STREAM II summer campaign in 1994, *Chemosphere: Global Change Sci.*, *1*, 233–248.

Wang, P., M. McCormick, L. Poole, W. Chu, G. Yue, G. Kent, and K. Skeens (1994), Tropical high cloud characteristics derived from SAGE II extinction measurements, *Atmos. Res.*, *34*, 53–83.

Winker, D., W. Hunt, and C. Hostetler (2004), Status and performance of the CALIOP lidar, *Proc. SPIE Int. Soc. Opt. Eng.*, *5575*, 8–15.

Zanis, P., et al. (2003), Forecast, observation and modelling of a deep stratospheric intrusion event over Europe, *Atmos. Chem. Phys.*, *3*, 763–777.

J. E. Barnes and M. O'Neill, Global Monitoring Division, NOAA, Boulder, CO 80305, USA.

U. Blum, Forsvarets Forskningsinstitutt, N-2027 Kjeller, Norway.

T. Deshler, Department of Atmospheric Science, University of Wyoming, Laramie, WY 82071, USA.

K. H. Fricke, Physikalisches Institut, Universität Bonn, D-53115 Bonn, Germany.

M. Fromm and E. P. Shettle, Naval Research Laboratory, Washington, DC 20375, USA. (mike.fromm@nrl.navy.mil)

M. Gerding, Leibniz-Institute of Atmospheric Physics, D-18225 Kühlungsborn, Germany.

H. Giehl and T. Trickl, IMK-IFU, Forschungszentrum Karlsruhe, D-82467 Garmisch-Partenkirchen, Germany.

T. Leblanc and I. S. McDermid, Table Mountain Facility, Jet Propulsion Laboratory, California Institute of Technology, Wrightwood, CA 92397, USA.

S. T. Massie, Atmospheric Chemistry Division, National Center for Atmospheric Research, Boulder, CO 80307, USA.

C. Ritter, Alfred-Wegener Institute for Polar- and Marine Research, D-14473 Potsdam, Germany.